THE PENNSYLVANIA STATE UNIVERSITY
SCHREYER HONORS COLLEGE

DEPARTMENT OF GEOSCIENCES

EARTHQUAKE PROCESSES IN THE LESSER ANTILLES SUBDUCTION ZONE

AUDREY DUNHAM
SUMMER 2017

A thesis
submitted in partial fulfillment
of the requirements
for a baccalaureate degree
in Geosciences
with honors in Geosciences

Reviewed and approved* by the following:

Charles Ammon
Professor of Geosciences
Thesis Supervisor

Maureen Feineman
Professor of Geosciences
Honors Adviser

* Signatures are on file in the Schreyer Honors

ABSTRACT

The Lesser Antilles Subduction Zone forms the eastern boundaries between the Caribbean - North American, and the Caribbean - South American Plates. No large earthquakes have struck along this active convergent boundary in recent history, but a Mw 7.5-8.5 megathrust event ruptured the northern segment of the boundary on 08 February 1843. In this study, 68 earthquakes greater than Mw 4.8 that occurred between 1982 and 2016 are relocated using a surface-wave cross-correlation method to improve the relative locations of the available moderate-magnitude seismicity. Using the improved relative centroid locations, we are able to better identify several fault orientations and spatial relationships. Analysis of the fault and slip orientations helps clarify some aspects of the regional stress regime along the arc and within the subducting North and South American Plates. An original motivation for this study was to better constrain the plate boundary between the North and South American plates. The available seismicity is insufficient to this task. Even with improved relative locations, the data are too sparse and the boundary definition remains diffuse. Six moderate-magnitude earthquakes of the Mw 6.3 21 November 2004 normal-faulting sequence between Guadeloupe and Dominica align along a single trend striking roughly 325°, consistent with the Global Centroid Moment Tensor (GCMT) faulting geometry estimates. Moderate-magnitude low-angle reverse faulting is common in the region (from Guadeloupe to the northern boundary), and is believed to have failed during the Great 1843 earthquake. The events are concentrated in the deeper segments of the plate boundary, but suggest a 120-130 km extent of seismogenic subduction in the 1843 segment. Seaward of the reverse faulting is a collection of strike-slip and oblique strike-strip (with a normal component) earthquakes, presumed to be in the subducting plate(s). These events

suggest northwest-southeast compressive stresses in the oceanic North American Plate, that rotate to a more north-south direction beneath the South American Plate. Strike-slip earthquakes closer to the arc suggest an east-west oriented compressive stress. These are likely in the upper plate (based on comparisons with nearby reverse faulting earthquakes), but the pattern is not uniform. A shallow event (GCMT depth of 5 km) from 2014 exhibits a northeast-southwest compression, similar to strike slip events to the east. The larger strike-slip events within the oceanic lithosphere produced few aftershocks, similar to intraplate (and transform faulting) earthquakes that occur within the oceanic lithosphere globally. The strike-slip events in the upper plate, although fewer in number, have more typical aftershock patterns. By compiling the data and observations from earthquakes along the Lesser Antilles Subduction Zone, we can better understand the faulting mechanisms and hazards in the region.

TABLE OF CONTENTS

LIST OF FIGURES

ACKNOWLEDGEMENTS

Thank you to my thesis supervisor, Dr. Charles Ammon, for the assistance and support he has given me throughout the year. From deciding on a topic to editing the final draft, he has been an amazing mentor and has helped me to become a better scientist. Thank you also to my honors advisor, Dr. Maureen Feineman, who has helped to keep me motivated and on track with my thesis. I would finally like to thank the Penn State Geoscience Department for their never-ending support of my endeavors and for giving me a home away from home.

Chapter 1

Introduction

The seismicity of the Lesser Antilles Arc has been studied extensively for many decades, but much remains to understand about the region in terms of both tectonics and seismic hazards. The North American and South American plates subduct obliquely beneath the eastern edge of the Caribbean plate at ~2cm/yr, which is relatively slow, especially given that the subducting lithosphere in the region is very old (~100my) (DeMets et al. 2000, 2010; Stein et al. 1982). The area is seismically active (Figure 1), with a few hundred small to moderate earthquakes each year, but has not hosted many earthquakes greater than magnitude 6; only 26 events since 1900 had magnitudes greater than or equal to 6 (Feuillet et al. 2011b, Hayes et al. 2013). The largest events shown in Figure 1 correspond to intermediate-depth events, which are a seismic hazard in this region, but my focus is on shallower events, which excite surface-waves more efficiently. The largest known earthquake in this region occurred on February 8, 1843 and is estimated to have a magnitude between Mw 7.5-8.5 and is almost certainly an underthrusting event. Other notable earthquakes occurred within the upper plate near Guadeloupe in 1867, the Virgin Islands in 1960, Antigua in 1974, and south of Guadeloupe in 2004 (Feuillet et al. 2011b). History has shown that the regional earthquake hazards include intraplate earthquakes in both the overriding and underthrusting plates, and of course, events along the plate boundary. Since no earthquake of comparable magnitude to that in 1843 has occurred since, the plate boundary has accumulated substantial strain and is capable of producing a significant earthquake (Hayes et al. 2013).

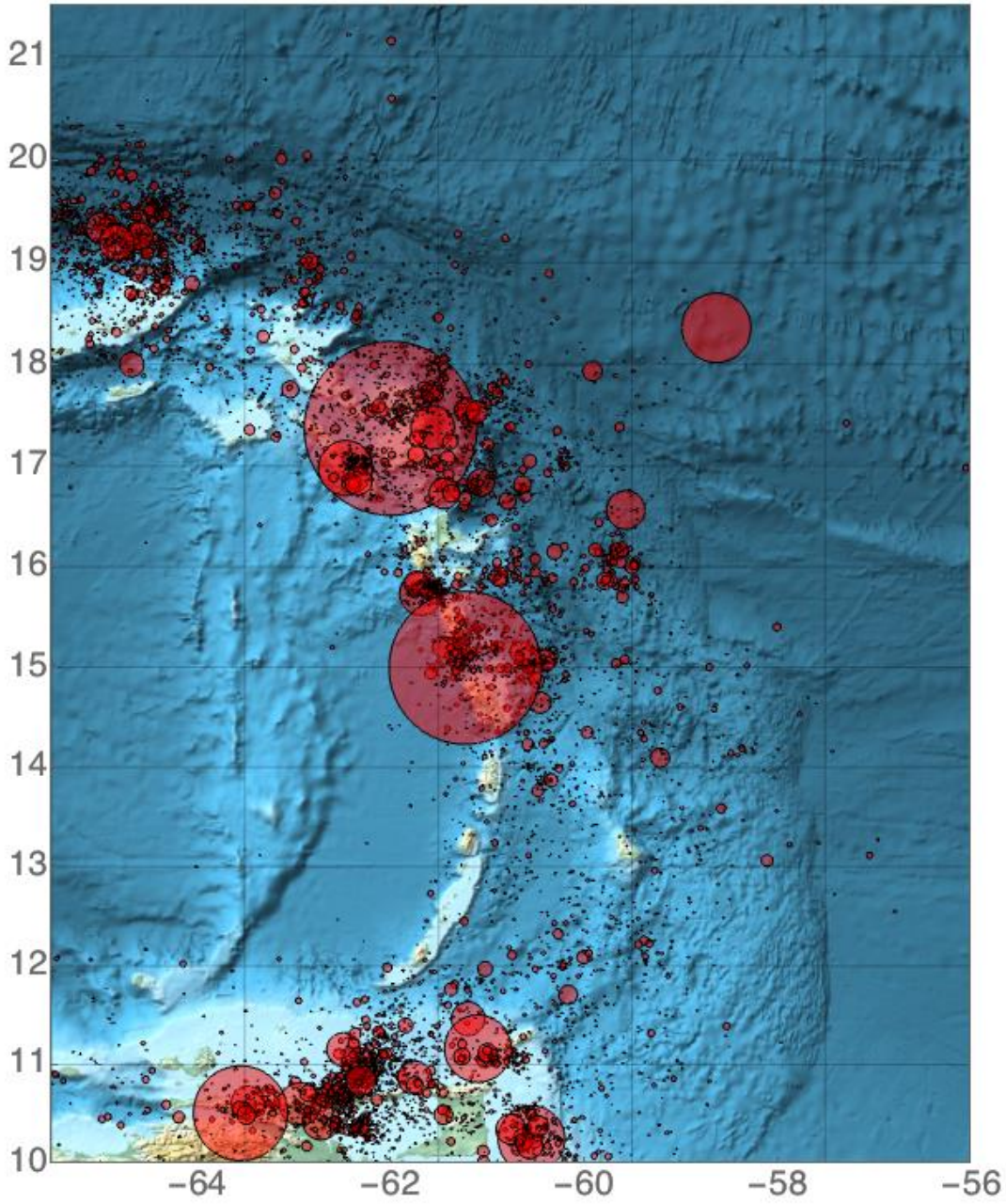

Figure 1 Seismic Map of the Lesser Antilles Arc

Figure 1. Earthquakes in the Lesser Antilles Subduction Zone region with magnitudes greater than 3.5 and occurring since 1970. Symbol area is proportional to seismic moment. Data source: The International Seismic Centre (ISC).

Hayes et al. (2013) concluded that the Lesser Antilles seismogenic zone has accumulated enough strain over the last 110 years to fail in a Mw ~ 8.2 ± 0.4. Using the estimated plate slip rate and assuming 100% coupling of the 1100 km long arc, the maximum magnitude (assuming the entire arc fails in a single event) is estimated to be Mw 8.95-9.58. An event this size has not been witnessed in history, but observations from other subduction systems suggest that earthquakes with M > 8.5 have recurrence times of ~500-1000 yrs. Such an event, although unlikely, cannot be discounted. In the past 10-15 years, we have seen two giant subduction earthquakes with unexpectedly high magnitudes, 2004 Sumatra and 2011 Tohoku. Both of these large earthquakes produced an accompanying tsunami that generally did more damage than the earthquake-induced shaking. The 1843 event did not produce a significant tsunami, but if the earthquake were to occur and include slip at shallow depths, a large tsunami could be excited and devastate the islands. If an event of Mw 8.95-9.58, or the size of the 1843 event, occurred today it would be exponentially more devastating than in 1843 due to the population increases on the islands in the past 40-50 years. Equally troubling is the fact that the region hosts roughly 500,000 daily beach visitors that have little to no knowledge of the tsunami and earthquake hazard (Hayes et al. 2013).

Given the potentially high consequences of a large event in the region, or a major earthquake in the vicinity of one of the more heavily populated islands, a review of recent moderate-magnitude seismic activity is warranted. In this work, I analyze 68 shallow earthquakes with Mw of 4.8 or greater that occurred since 1982 and are located in the region bounded by 10N and 20N and -58W and -66W. The magnitude threshold is defined by the need to know the faulting geometry of the earthquakes, which for these size events can be obtained from the GCMT catalog. To ensure that we have sufficient digital seismic data for the events, I

work with earthquakes that have occurred since 1980. The data from more recent events is much more complete, and so the results are weighted toward the present. To facilitate a comparative analysis, the earthquakes are divided into strike-slip, normal, and reverse faulting earthquakes that can be relocated (relative to each other) using relative time shifts measured using cross-correlated surface waves. More precise locations can provide more insight into the fault systems hosting the seismic activity. One of the original targets for the analysis was to better define the boundary between the North American and South American plates, which is not well known in the region. Unfortunately, the sparseness of events prevents me from better delineating this important structure. I also explored P-waveforms to refine earthquake depths in an attempt to better image the subduction interface and depth of intraplate deformation in both the subducting and overriding plates. Finally, I used the geometric information on faulting obtained as part of the GCMT project to explore first-order variations in stresses in the interacting plates.

Chapter 2

Tectonic Setting

The Lesser Antilles Arc formed as a result of the subduction of the Atlantic Ocean floor beneath the eastern margin of the Caribbean Plate. Along the arc, the Lesser Antilles Subduction Zone (LASZ) forms the plate boundary between the Caribbean and the North American plates to the north and the Caribbean and South American plates to the south. The precise boundary between the North American and South American plates is unknown, but given the relative motion expected between the plates in this area, it is believed to be a transform boundary located between 10N-20N (Dorel 1981, Stein et al. 1982). The North American and South American plates subduct obliquely beneath the Caribbean Plate, producing the volcanically active island arc and one of the broadest accretionary prisms in the southern hemisphere. Global plate models suggest that the relative motion between the Caribbean and North American plates and between the Caribbean and South American plates is similar with the oceanic plates moving ~2 cm/yr in WSW direction (DeMets et al. 2010) relative to the Caribbean Plate (Figure 2). Since the motion between the North American and South American plates accommodates a low rate of relative motion, it is very difficult to determine any modest convergence between the two (Hayes et al. 2013). The down-dip limit of the seismogenic zone has been constrained to about 45 km depth and estimates of the down-dip width of the plate boundary are roughly 120 km. Even with this low rate of motion, the LASZ accumulates strain per kilometer-of-arc each year equivalent to a Mw 5.4 earthquake (assuming a shear modulus of 45 GPa, a down-dip width of 120 km, and 100% coupling (Dziewonski & Anderson 1981, Hayes et al. 2013). Integrating that strain

accumulation rate over 300 km of the arc (an estimate of the LASZ boundary length given by Feuillet et al. 2011b), equates to accumulating strain equivalent to a Mw 7.0 each year. The result suggests that significant strain may have accumulated in the region since the 1843 earthquake (Feuillet et al. 2011b, Hayes et al. 2013). The exact strain accumulated depends on the seismic coupling estimates – assuming 100% coupling provides a maximum bound for a large earthquake size, but boundary coupling is unlikely complete along the whole arc (Laigle et al. 2013).

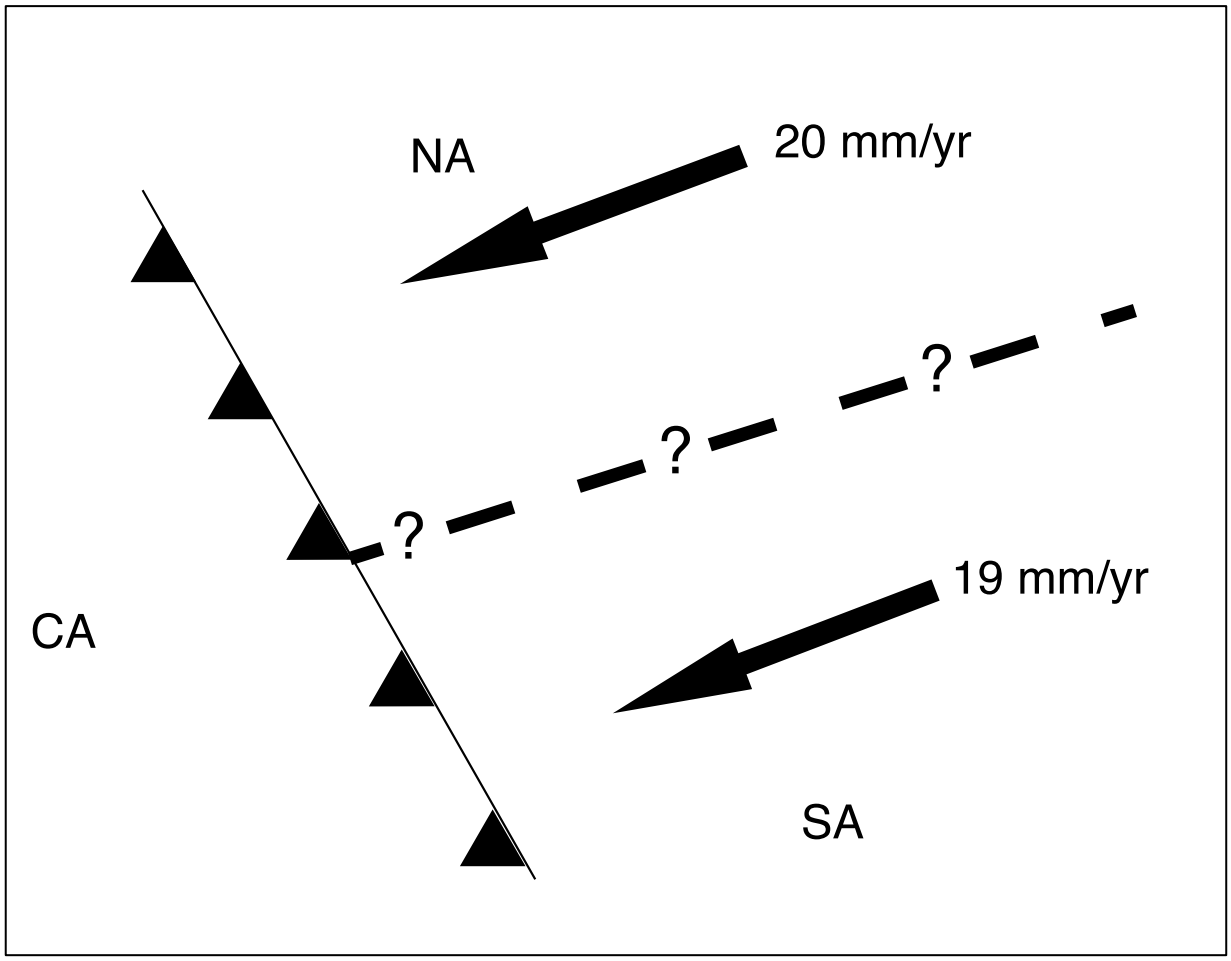

Figure 2 Tectonic Plate Motions

Figure 2 The plate motions between the Caribbean (CA), North American (NA), and South American Plates are shown in this figure. The dashed line denotes the unknown location of the NA/SA plate boundary. The plate motions are calculated using the UNAVCO plate motion calculator with a MORVEL 2010 plate motion model at 15N and -61S. The Caribbean plate is used as the stationary reference frame.

As mentioned above, the LASZ accretionary prism is unusually thick and well developed, particularly south of 15N (Figure 1). Other key bathymetric features include several northwest-southeast oriented aseismic ridges. The Barracuda ridge, located offshore of Guadeloupe, and the Tiburon Rise, located offshore Martinique, are parallel bathymetric highs that rise ~2 km above the sea floor, and are associated with negative gravity anomalies (Stein et al. 1982) (Figure 3). Because hot spot traces leave a positive gravity signature, it can be inferred that these are flanking ridges originating from the Mid-Atlantic Ridge (Laigle et al. 2013, Stein et al. 1982). The Barracuda Ridge strikes N288E and the Tiburon Rise strikes N294E, both oblique to the arc. Subduction of ridges is an important process in most subduction zones. We do not know whether these ridges impede or enhance seismicity in the LASZ, but the issue has been long debated since bathymetric highs may cause boundary segmentation and affect the propagation of earthquake ruptures. McCann and Sykes (1984) proposed that the 1843 earthquake rupture might have been bounded by trenchward extensions of the Barracuda Ridge and Tiburon Rise. This may be the case, but Laigle et al (2013) note that the aseismic ridges did not prevent the whole arc from rupturing in the 2011 Tohoku earthquake (Hayes et al. 2013, Laigle et al. 2013). The general connection between seamount and ridge subduction and seismicity has been debated by McCann and Sykes (1984, 1986) and Stein et al. (1986) and others. Wang and Bilek (2011) suggested that it would be probable for these subducting bathymetric highs to produce aseismic creep rather than large propagating ruptures. Although the interaction of bathymetric ridges with subduction has been extensively studied, the consequences remain only locally constrained.

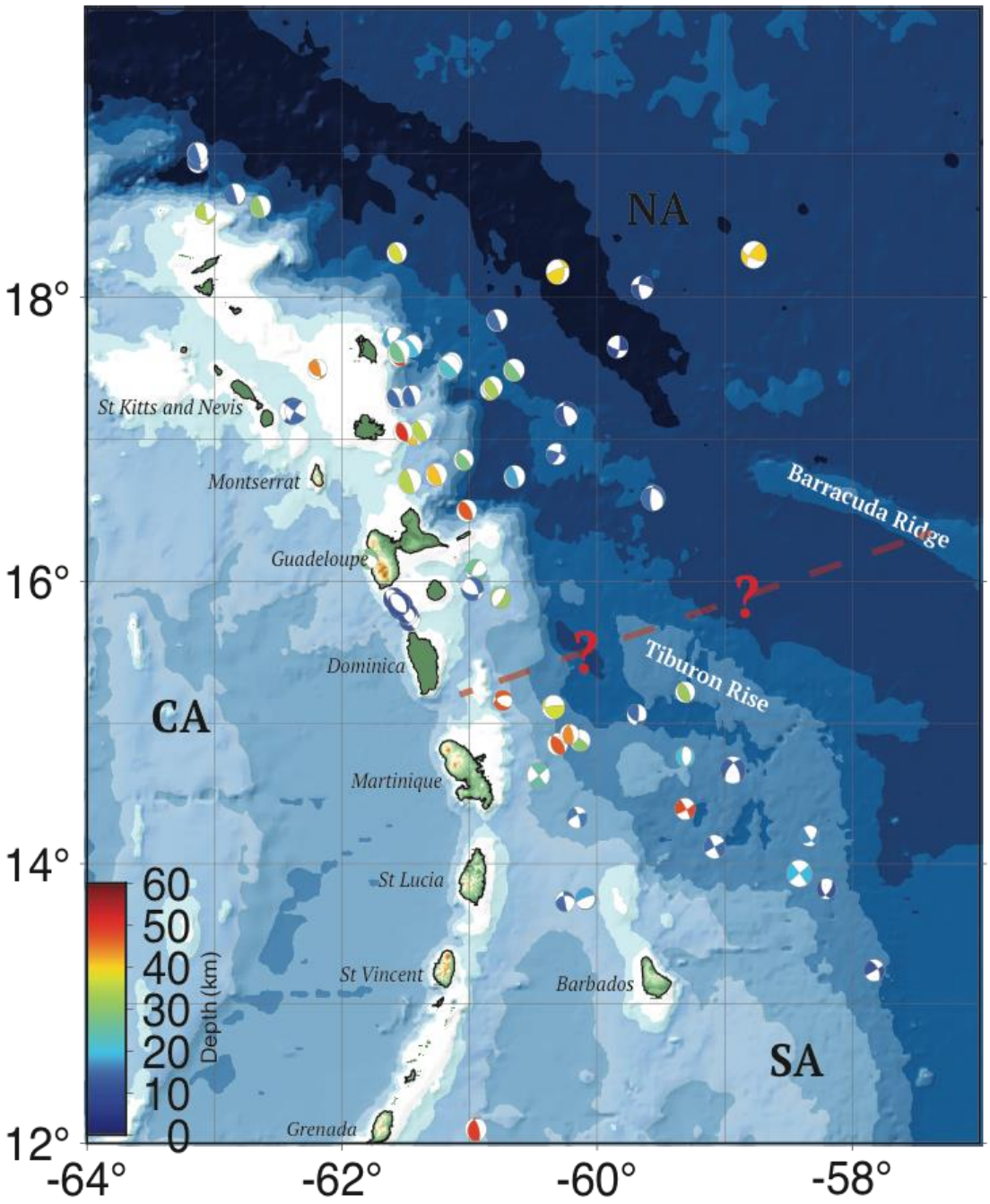

Figure 3 Earthquakes analyzed in this study

Figure 3. The 68 earthquakes of this study are shown here with focal mechanisms colored for depth. The Barracuda Ridge, Tiburon Rise, and islands along the arc are labeled. The Caribbean (CA), North American (NA) and South American (SA) are also labeled. The dashed red line shows a potential boundary between the North and South American plates and is indicated with question marks because the actual location is not known.

Chapter 3

Regional Seismicity

The Lesser Antilles Arc has been studied since the mid-1900s. Dorel (1981), Stein et al. (1982), McCann & Sykes (1984), Bernard & Lambert (1988), Feuillet et al. (2011), and Hayes et al. (2013), have all examined past seismicity and the seismic hazards associated with the LASZ. Seismic instrumentation of the Lesser Antilles began with the first permanent seismometer installed in Martinique in 1936 (Dorel, 1981). Today, a vast seismic network including permanent and temporary seismic stations has been built to monitor and study the regional seismicity. Although the detection of local seismic events began in 1936, we have information on earthquakes dating back to 1690 through historic accounts. The LASZ is a seismically active region, hosting a few hundred felt earthquakes every year. Although earthquakes are common, large shallow earthquakes are infrequent, only five earthquakes with $M \geq 6$ and shallower than 70 km, have occurred in the past 35 years. The total seismicity of the arc with $Mw \geq 4.8$ since 1977 is shown in Figure 4. Assessing the regional seismic hazards requires that we combine information on recent and historic earthquakes.

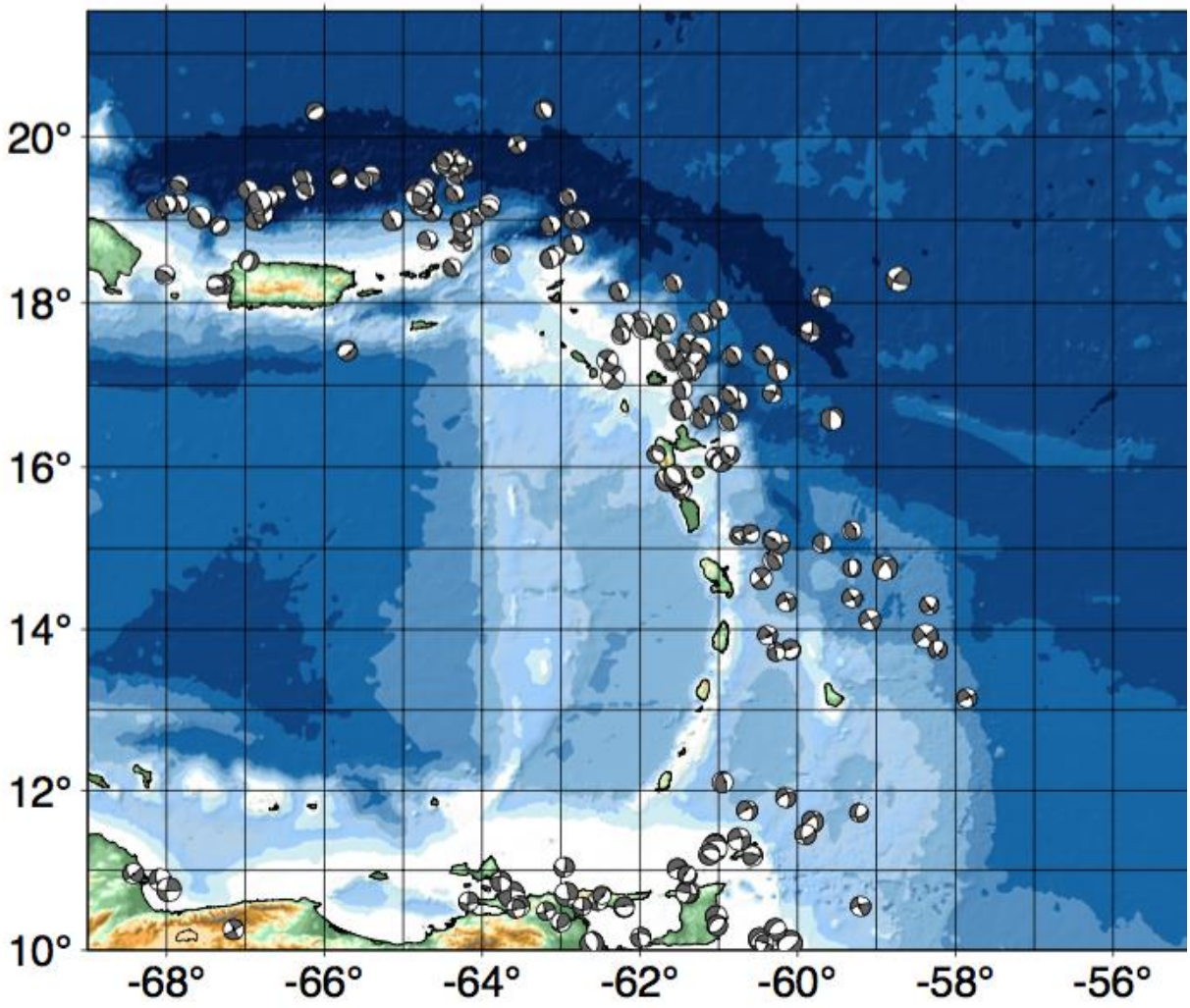

Figure 4 Seismicity since 1977

Figure 4. Image of the focal mechanisms of earthquakes throughout the arc of Mw ≥ 4.8 since 1977.

The results of a Gutenberg-Richter magnitude-frequency analysis of the events in Figure 1 are presented in Figure 5. The analysis spans a 45-year period and the data show a clear linear pattern between the logarithm of the number of events and the magnitude. The b-value (negative of the slope of the line) of the distribution is 1.0 and on average there is an event with $M \geq 7$ about every 20 years. Assuming a b-value of unity, this would forecast an event of magnitude 8 every few hundred years. The distribution of magnitudes with time is shown in Figure 6 and the distribution of magnitudes with latitude is shown in Figure 7.

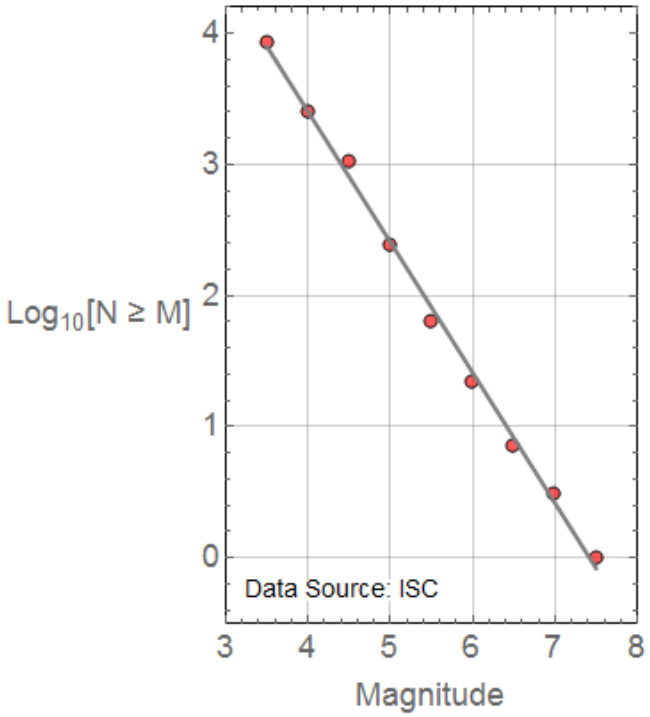

Figure 5 Gutenberg-Richter Relationship

Figure 5. An image of the Gutenberg-Richter relationship for earthquakes of magnitude 3.5 and above for the Lesser Antilles Arc.

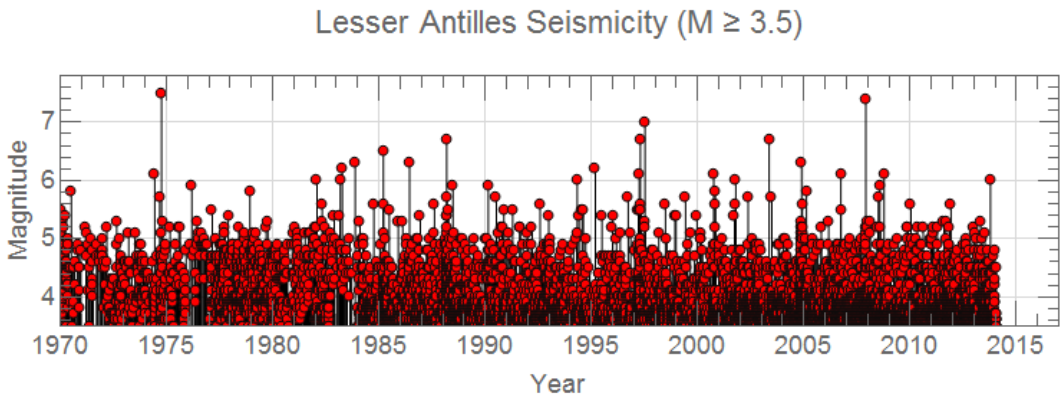

Figure 6 Seismicity distribution through time

Figure 6. Distribution of seismicity with time and magnitude throughout the Lesser Antilles arc, Mw >3.5 since 1970.

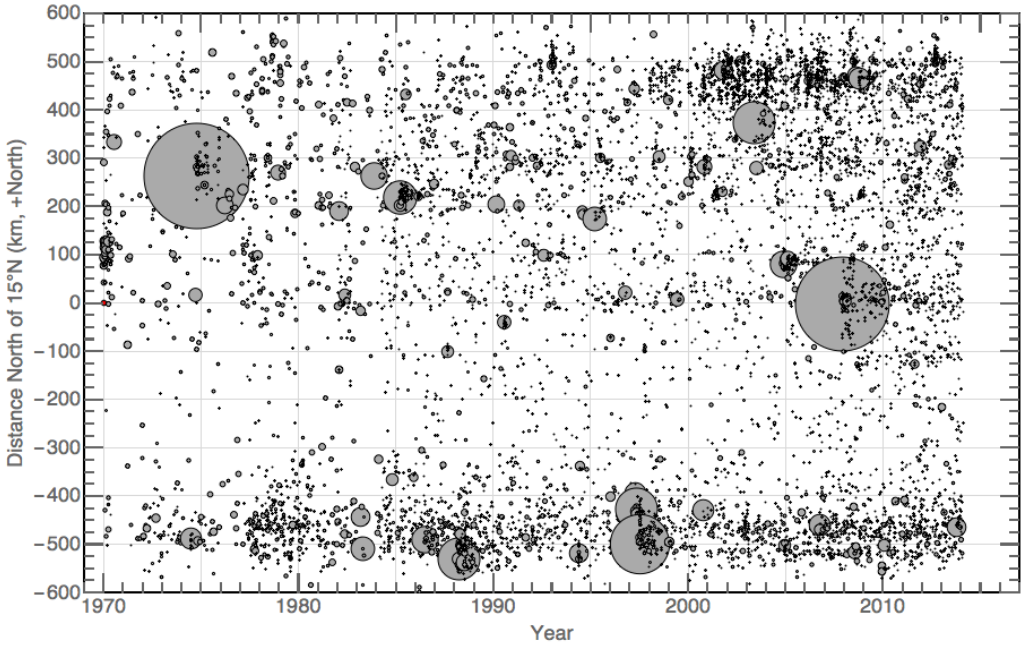

Figure 7 Spatial and temporal frequency of seismicity

Figure 7. Distribution of earthquakes through space and time with a 15N reference position. Earthquake symbol size is scaled with seismic moment. High densities of earthquakes to the south integrate activity along northern South America rather than along the LASZ.

Chapter 4

Historic Seismicity

Historic seismicity can inform a discussion of the regional seismic hazard, and in this case, provide much needed information from the times prior to local seismic monitoring. The 08 February 1843 event was the most damaging earthquake in the recent past and due to the fact that no other earthquake has ruptured this area since, the area of that rupture poses the greatest threat to the arc. Megathrust earthquakes are responsible for the majority of earthquake hazard throughout the world, causing the most damage through shaking as well as tsunamis, if they are located offshore, as was the case for the 1843 event. Through combining historic and current records, Hayes et al (2013) determined that there is a possibility of a Mw ~8.2 in the seismogenic zone that has a dip of 14°, a down dip width of 120 km, and a length of 120 km. This could also produce a tsunami with a maximum wave height of 3 m at the Guadeloupe Archipelago (Hayes et al. 2013). Figure 8 is a map of the historic ruptures from the Lesser Antilles reviewed in this section. I focus on notable events of the region that are used to place some of my own results in context.

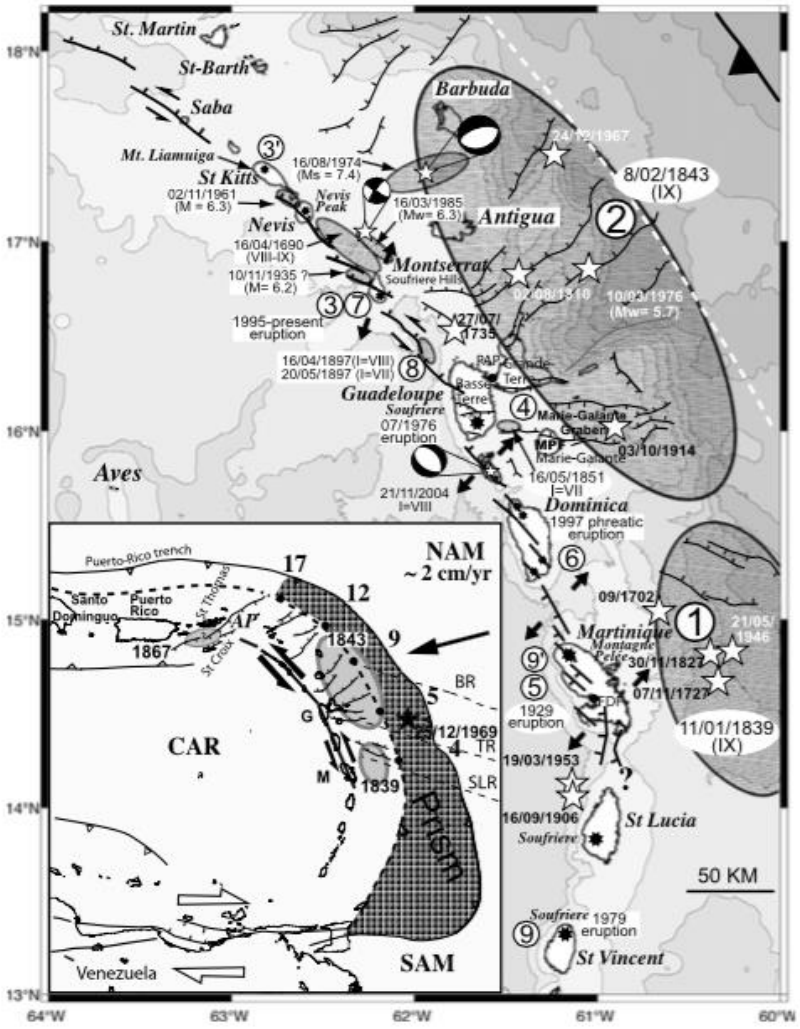

Figure 8 Historic Seismicity Map

Figure 8. Map of the historic ruptures correlating to the events described in this section. The largest earthquake is the Mw 7.5-8.5 08 February 1843. Figure from (Feuillet et al. 2011b).

April 16, 1690

This is the earliest, large reported earthquake in the LASZ. Damage was reported in Antigua, St. Kitts, and Nevis. A conflicting report states that an earthquake was felt on April 5 and then more on the 10th and 16th. Maximum intensity was around VIII. Some consequences of this event were a 3 m wide, open fissure in St. Kitts and a landslide at Nevis' Peak. The event was most likely accompanied by a tsunami as witnessed by the withdrawal of the sea by 200 m. It is thought that this event ruptured in the Montserrat Havers and Redonda en echelon fault system (Feuillet et al. 2011b), faults identified using bathymetric and seismic reflection profiles.

January 11 1839

This event destroyed Fort Royal and killed several hundred people. The maximum intensity was around VIII and IX. Intensities from other islands suggest that the epicenter was east of Martinique. The event was most likely a megathrust rupture, similar to the 08 February 1843 event (Feuillet et al. 2011b).

February 8 1843

This event is the largest reported earthquake in the Lesser Antilles Arc in the past 300 years, estimated to be a Mw 7.5-8.5 (Bernard & Lambert 1988, Feuillet et al. 2011b). The city that was most affected by this event was Pointe-à-Pitre in Guadeloupe, which was almost completely destroyed (Bernard & Lambert 1988, Feuillet et al. 2011b, Laigle et al. 2013). There were 1000-1200 deaths, a very large toll in comparison to other districts on Guadeloupe with only 50 deaths or less. The shaking was not worse in this region, but a fire due to the earthquake is the main cause of death as well as destruction of the city (Bernard & Lambert 1988, Feuillet et

al. 2011b). This event is thought to be a megathrust that ruptured between about 16N to 18N and is estimated to have a rupture length between ~100-300 km (Bernard & Lambert 1988, McCann & Sykes 1984). Hydrologic phenomenon on the Grande-Terre and Basse-Terre associated with this event included mud fountains 1.5 m high, liquefaction, and the appearance and disappearance of springs (Bernard & Lambert 1988, Feuillet et al. 2011b). Landslides and cliff collapses were also induced as seen in the wharfs at Pointe-à-Pitre subsiding approximately 3 cm. Felt aftershocks lasted for more than 8 months and had maximum intensity ranges from III-VIII in Guadeloupe (Feuillet et al. 2011b). The only account of a possible tsunami was a report of the sea rising 4 ft but then immediately falling again (Bernard & Lambert 1988). A possible explanation for the lack of tsunami from this large earthquake could be that it was located at a deeper region of the megathrust plate interface (Feuillet et al. 2011b, Hayes et al. 2013).

May 16 1851

The 1851 event was a maximum intensity VII event that most likely ruptured a segment of the Mome-Piton normal-fault system between Marie-Galante and Basse-Terre (Feuillet et al. 2011b).

April 29 1897

This rupture might locate between the 1690/1985 and 2004 earthquake ruptures along the southern part of the Bouilante-Montserrat fault segments. The 1897 event had intensities of VIII in Guadeloupe and is estimated to have a magnitude of either a 5.5 or 7. Serious damage at Pointe-à-Pitre resulted in 4 deaths (Feuillet et al. 2011b).

November 10 1935

The 1935 event was a M 6.2 intermediate depth earthquake (depth ~100 km) within the North American slab. This is the first earthquake in this list known from data rather than historical reports. Intensities among the surrounding islands varied from III to VIII (Feuillet et al. 2011b).

December 29 1950 and November 2 1961

A series of earthquakes struck the islands of Nevis and St Kitts in the northern LASZ on 29 December 1950 and continued until May 1951. Over 150 earthquakes occurred in January of that year. Ten years later, another series of earthquakes occurred, with the 02 November 1961 event the strongest. The sequences most likely occurred on a NW-SE dipping en echelon fault system (Feuillet et al. 2011b).

Christmas Day 1969 Sequence

A major earthquake sequence began on Christmas in 1969 and continued into early January 1970. These events were unusual in that they located east of the trench and east of any other earthquakes. The focal mechanisms of these events were evaluated in Stein et al. (1982) who found that the mainshock was a normal faulting event striking N-S with a Ms of ~7.5. The aftershocks were a combination of strike-slip and normal faulting events (Stein et al. 1982).

October 8 1974

Surface-wave magnitude estimates for the 1974 earthquake range from Ms 7.1-7.6. From the analysis of aftershocks, Feuillet et al. (2011b) suggested that the rupture was within the overriding Caribbean plate on a southeast dipping normal fault. The largest event occurred at 30km depth, most likely on the well-mapped arc-perpendicular normal faulting system northeast of Guadeloupe.

March 16 1985 and November 21 2004

Together with the Mw 7.4 on 29 November 2007, the 1985 and 2004 events are two of the largest events recorded in the Lesser Antilles in the past 35 years. Both earthquakes had a Mw 6.3 and are intraplate events that ruptured parallel to the arc. The 16 March 1985 event caused damage in Point-à-Pitre with an intensity of VI and ruptured on a NW-SE striking strike-slip fault. The 21 November 2004 ruptured a 325° striking normal fault with intensities of IV on Martinique and between IV and VIII on Guadeloupe (Feuillet et al. 2011b).

Chapter 5

Methods

Surface-Wave Based Relative Earthquake Relocation

Earthquake locations in the USGS-NEIC catalog are constrained primarily by seismic P- and S-waves (body waves) and events are located individually as they occur. Earthquakes can be accurately located using body waves in dense seismic networks, but when an earthquake occurs in a region with few seismometers, such as offshore, it is more difficult to locate the events accurately and precisely using body waves. For non-real time location, seismologists have developed approaches to locate more than one event at a time, using information from clusters of earthquakes to improve the relative locations of the events and at times, the absolute locations of smaller events that are constrained by fewer observations (Shearer 2009, Stein & Wysession 2003). In this study, I employ a more precise method of calculating relative event locations, outlined in Cleveland and Ammon (2013), that utilizes surface wave cross-correlations to estimate time shifts that constrain relative earthquake locations. Using surface waves to relocate events based on relative distances to other earthquakes in the region has advantages in offshore regions like the LASZ. Surface waves have a low propagation speed, which makes the time delays for location differences large enough to measure precisely and allows earthquakes to be located precisely. P-waves have higher phase velocities, which produce smaller time shifts for the same event offset distance. For example, a location difference of 16 km may produce a time shift of 5.0 s for surface waves, but shift P-waves only about 1.0 s. Unless high-frequencies are

available to measure the P-times more precisely, the surface waves are more sensitive to the locations.

To perform the relocations, seismograms were downloaded from the IRIS Data Management System using the *obspy* Python package for seismic analysis (Krischer et al. 2015). Rayleigh waves are isolated using the catalog location and origin time and a 5-3 km/s group velocity window. The quality of individual seismic signals was assessed by visual inspection of each seismogram. Love and Rayleigh waveforms of each event were graded A through F based upon signal-to-noise ratio. If a waveform exhibits high signal-to-noise ratio it is given an A, but if it has a low signal-to-noise ratio it is given a D. Seismograms from sensors that show obvious instrument problems (no signal, no signal variation, large glitches, etc.) are assigned a quality F. Only waveforms graded A through C are used to compute cross-correlations for the location analysis.

Cross-correlation is a measure of waveform similarity. For similar shaped waveforms, I measured the optimal time shift (identified by the maximum in a time-varying cross-correlation function). To avoid issues associated with time shifts resulting from differences in faulting geometry, I analyzed reverse, normal, and strike-slip faulting events in three separate inversions. To ensure that only the highest quality signals are used in the locations, a minimum normalized (to ±1) cross-correlation threshold of 0.9 is used. In other words, waveforms of two different events must have a similarity above 0.9 in order to be linked (used in the location). We also restrict signal linking to events no farther than 180 km apart, and only link events for which at least 12 waveforms with a cross-correlation above 0.9 exist. Utilizing a high cross-correlation can reduce nodal effects from the phase differences between events (Cleveland & Ammon, 2013). Example event-pair cross-correlations are shown in Figures 9 and 10. Each symbol

represents a pair of waveforms (one from each event) observed at a single station. The top panel shows the azimuthal differential travel time pattern, which should resemble a sinusoid for a simple spatial offset. The amplitude of the sinusoid is proportional to the distance between the events and the average value of the sinusoid represents the difference in centroid times between the two events and the original origin times. The top inset summarizes the initial and final relative location information. The events corresponding to Figure 9 are close together (small amplitude sinusoid) and were relocated to be closer together and to have a nearly opposite azimuthal relationship as the original locations. However, azimuthal resolution for close events is difficult to resolve since a small shift in relative position of nearby events can change their azimuthal relationship dramatically. The events corresponding to Figure 10 are roughly 75 km apart and the sinusoidal parameter is greatly enhanced. The origin time shift in this case is roughly 2 seconds.

I attempted to apply the surface-wave relocation procedure to 68 shallow earthquakes that occurred in the Lesser Antilles region during the years from 1982 to 2016. As is usually the case, not all events had sufficient data and similarity to be relocated. In this instance, 42 out of the 68 events were relocated, and the results are discussed below.

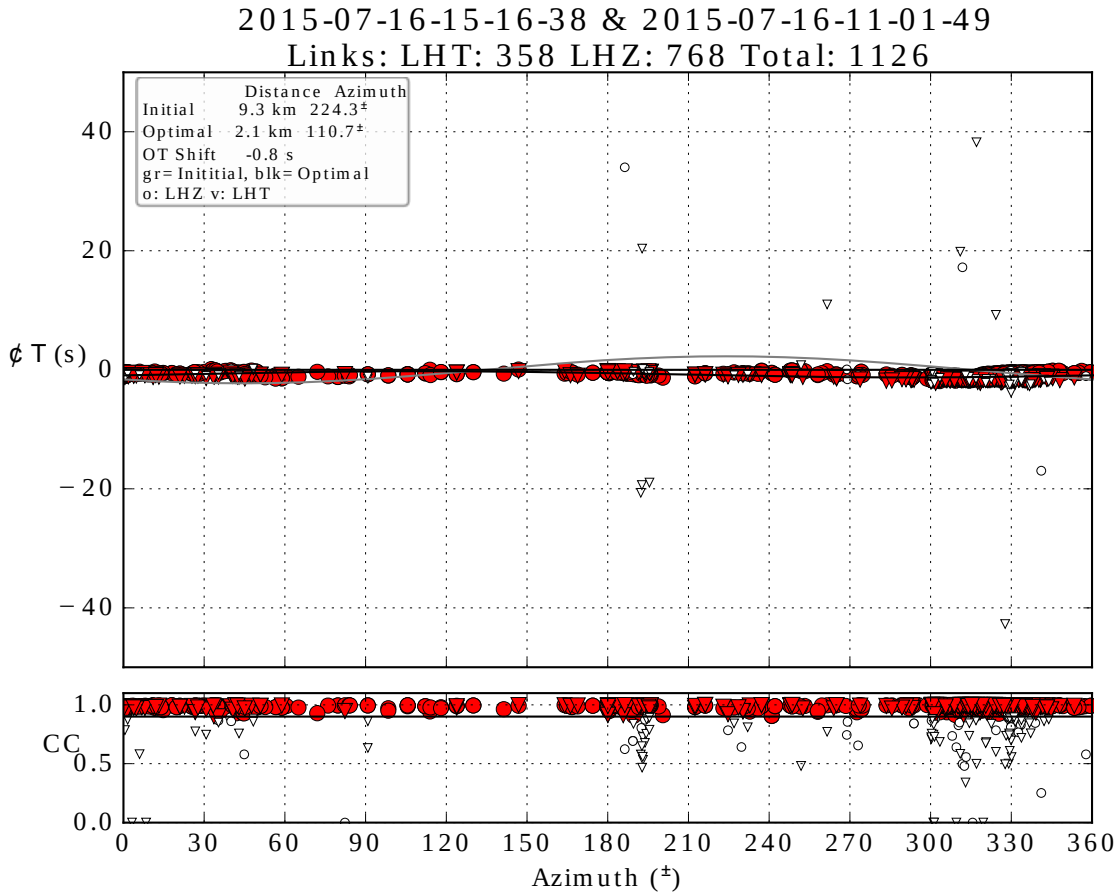

Figure 9 Cross-correlation curve for two strike-slip faulting earthquakes

Figure 9. The top panel shows optimally estimated (black curve) and original-location predicted (gray curve) time shifts as a function of the source-to-station azimuth. The lower panel shows the cross-correlation values for the same data. Red symbols identify signals with peak correlations that meet or exceed 90% (thin black line in lower panel), gray outlined symbols identify events that did not meet correlation criteria and were not used in the locations. The top panel also includes best-fit cosine curves for the initial and final relative event location. LHT indicates a Love-wave observation, LHZ indicates a Rayleigh-wave observation. OT Shift indicates a mix of origin time and centroid time shifts. See text for discussion.

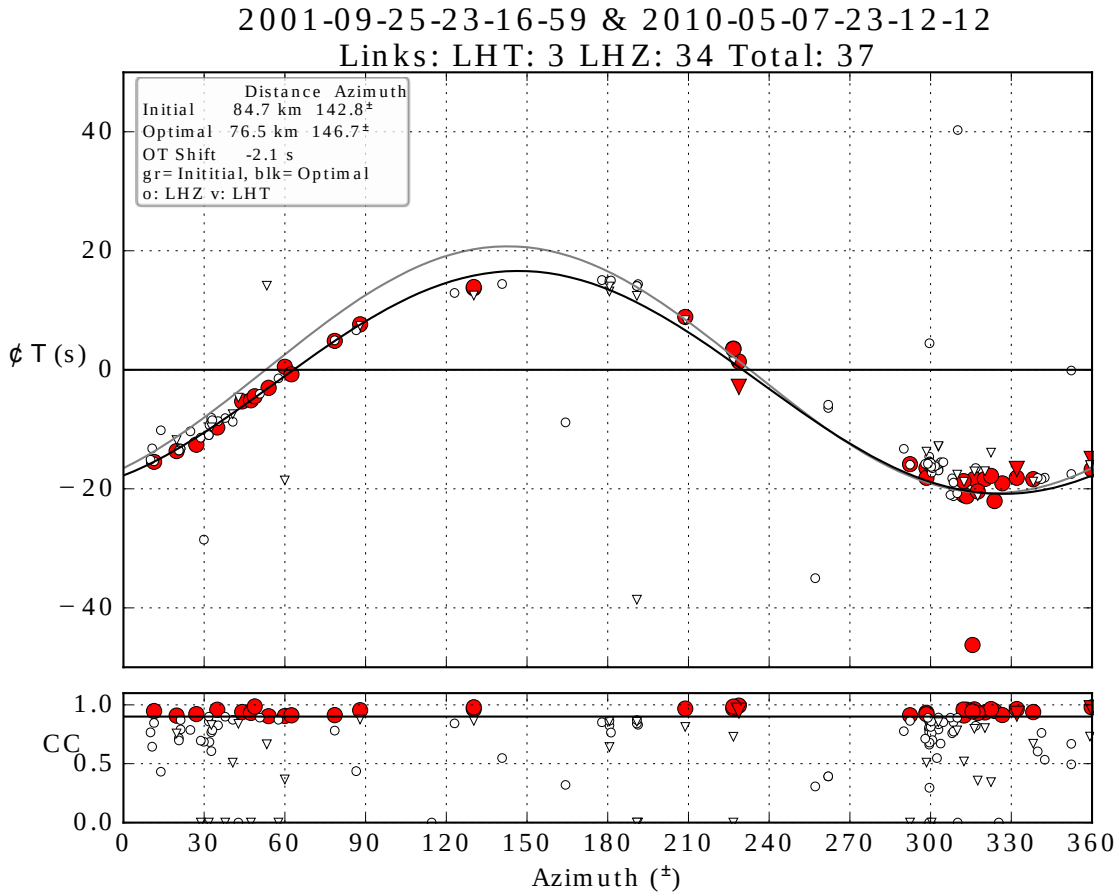

Figure 10 Cross-correlation curve for two reverse faulting earthquakes

Figure 10. The top panel shows optimally estimated (black curve) and original-location predicted (gray curve) time shifts as a function of the source-to-station azimuth. The lower panel shows the cross-correlation values for the same data. Red symbols identify signals with peak correlations that meet or exceed 90% (thin black line in lower panel), gray outlined symbols identify events that did not meet correlation criteria and were not used in the locations. Top panel also includes best-fit cosine curves for the initial and final relative event location. LHT indicates a Love-wave observation, LHZ indicates a Rayleigh-wave observation. OT Shift indicates a mix of origin time and centroid time shifts. See text for discussion.

Body Wave Modeling For Earthquake Depth Estimation

The surface-wave locations only provide information on the latitude and longitude of the event spatial centroids. An equally important location parameter is the spatial centroid depth. To provide information on the event depths, I used a P-waveform modeling procedure that is often used on moderate and large earthquakes (Langston & Helmberger 1975, Stein & Wysession 2003). Since teleseismic P-waves from strike-slip events are near nodal, and generally complicated, I focused on reverse-faulting events. I assumed a simple half-space earth model with a six-kilometer thick water layer above. The half-space P-wave velocity was 6.5 km/s (an average for oceanic crust). I assumed the faulting geometry from the GCMT catalog solutions and filtered the signals to improve signal-to-noise ratios in the shorter periods (which are the only frequencies above noise for the smaller events). I adjusted the event depth to produce a match to the waveforms. I applied the procedure on nineteen events but the confidence in the fits using such a simple model and the available bandwidth is low and therefore I will not discuss the results further. A table of my depth estimates is provided in Appendix A.

Chapter 6

Results

Figure 11 is a map of the 42 original epicenters (yellow circles) and relocated epicentroids (focal mechanisms). The original epicenters and relocated earthquake epicentroids are tabulated in Appendix B.

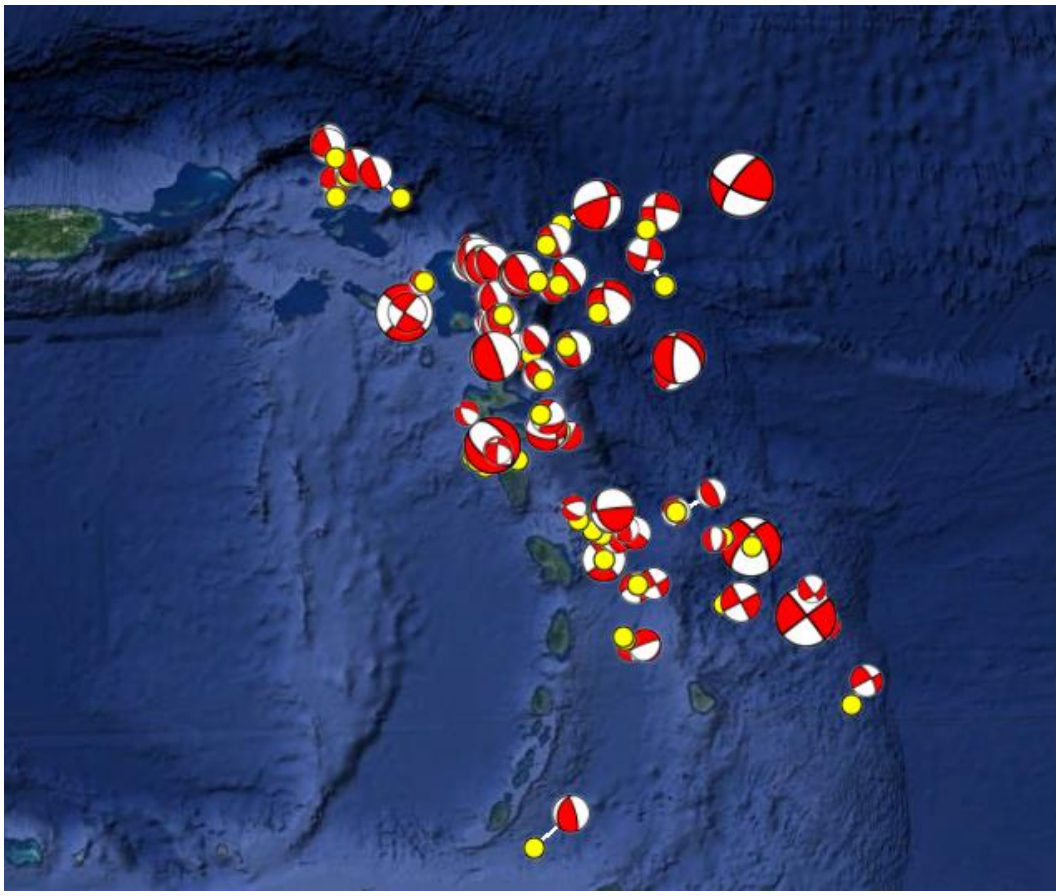

Figure 11 Earthquake Relocations

Figure 11. Lower-hemisphere focal mechanisms of the relocated events are centered in the surface-wave epicentroid locations and the original epicenters are shown as yellow circles. Original and final locations are connected by the white lines, and the focal mechanisms are scaled to indicate earthquake relative magnitude. The width of the image is ~1,000km. Image from Google Earth.

Normal-faulting earthquake relocations

Nineteen normal-faulting earthquakes were cross-correlated and 11 of those events linked and were relocated. The average distance from the initial epicentroid of the NEIC to the final epicentroid is 8.7 km and ranges from 5 km to 55 km. The absolute centroid time shifts range from 0 s to 22 s with a mean of 0 s. Mean absolute misfit of the double difference residuals changed from 3.45 s before relocation to 0.60 s after relocation. The normal-faulting events are distributed around the study region, but an interesting cluster (A) is located in near 16N and between -62W and -61W. This cluster is discussed at length in the discussion. Summary statistics from the relocations are shown in Appendix B.

Reverse-faulting earthquake relocations

Of the 33 reverse-faulting earthquakes I analyzed, 21 linked and were relocated. The distance from the initial NEIC epicenter locations to the final epicentroid relative relocations ranges between 5 km and 66 km, with an average shift of about 16 km. The absolute centroid time shift from the original NEIC origin time to the final relocation time is between 0 s and 6 s, with an average of 0 s. The mean absolute double difference residual misfit was initially 5.3 s and was 1.1 s after relocation. Most of the reverse-faulting events are located directly east of the northern arc segment. These events are likely interplate earthquakes and therefore may provide insight into the seismogenic zone of the subduction zone. Other reverse-faulting event clusters are to the north (H) and the south (G) that may relate to stress changes within the arc. Summary statistics are shown in Appendix B.

Strike-slip faulting earthquake relocations

Of the 16 strike-slip faulting events that I analyzed, 10 linked and were relocated. The shift of the epicentroid from the NEIC epicenter ranged from 5 km to 10 km, with a mean shift of 4.5 km. The absolute time shift ranged from 0 s to 3 s with an average of a 1.1 s shift. The initial double difference residual was 1.55 s for the NEIC locations and 0.54 s following relocation. The strike-slip events are spread sparsely across the region but appear to provide some insight into the stress changes between the subducting and overriding plate. The main clusters of strike slip events are located to the east of the arc in the north and south. Location summary statistics are shown in Appendix B.

Chapter 7

Discussion

To explore the relocations and their implications, earthquakes with similar characteristics (faulting geometry, location) are clustered and discussed group-by-group. The clusters are defined in Figure 12 and range from a broad region of underthrusting (D) to quite small two-event clusters that represent a mainshock and aftershock.

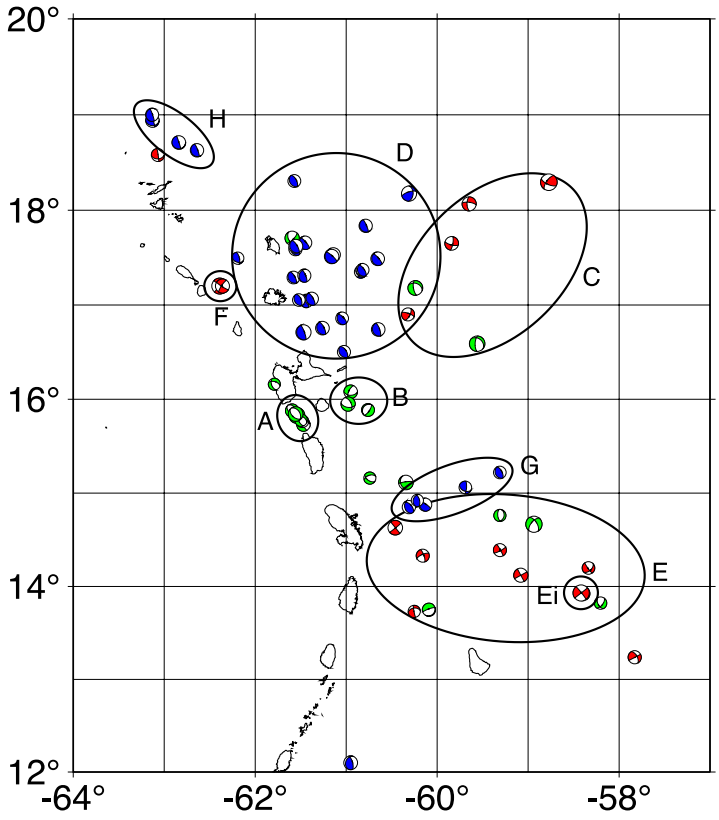

Figure 12 Map of earthquake clusters

Figure 12. Definition of the earthquake clusters discussed in the text. The events were grouped by spatial relationship and focal mechanism type (stress regime). The colors indicate faulting mechanism, normal (green), reverse (blue), strike-slip (red)

Cluster A

Cluster A consists of six normal faulting events, three of which occurred on 21 November 2004, two events occurred days later, and one roughly two months later (Figure 13). The cluster is a mainshock-aftershock sequence. The largest earthquake, the Les Saintes earthquake, was a Mw 6.3; the largest aftershock was the last event analyzed in the sequence, a Mw 5.8 that occurred two months later. I sampled only the largest events in the aftershock sequence (those that had GCMT solutions). Local and regional monitoring detected over 30,000 smaller aftershocks that continued from 2004 into 2008. Most are located near the Guadeloupe Archipelago and occurred at shallow depths (Feuillet et al. 2011a). The main shock caused much damage on Les Saintes island, one fatality in Guadeloupe, and a small tsunami (Feuillet et al. 2011a). The aftershocks did not migrate in one direction, but expanded outward from the main shock along a known normal fault (the Roseau fault) with an orientation of ~325°. The Roseau fault is part of the en echelon Les Saintes Fault system (Figure 14, Bazin et al. 2010). The GCMT solution for the mainshock and the Roseau fault have very similar strikes, 325° (GCMT) and 315°, and the Roseau fault is approximately 15-20 km long, similar in length to the aftershock sequence (Bazin et al. 2010). One of the earthquakes originally in the clusters shifted north of Les Saintes, but the three earthquakes to the north in the cluster have a similar strike matching the Roseau fault and align along the same direction. The three events in the cluster to the south suggest more variable faulting geometries and may reflect the increase in en echelon faulting in the southern part of the Les Saintes Fault System. The overall length of the region participating in the moderate-magnitude activity is about 20 km, consistent with the overall

aftershock length. Our locations for the largest aftershock and the mainshock differ by less than five kilometers, with the aftershock to the north.

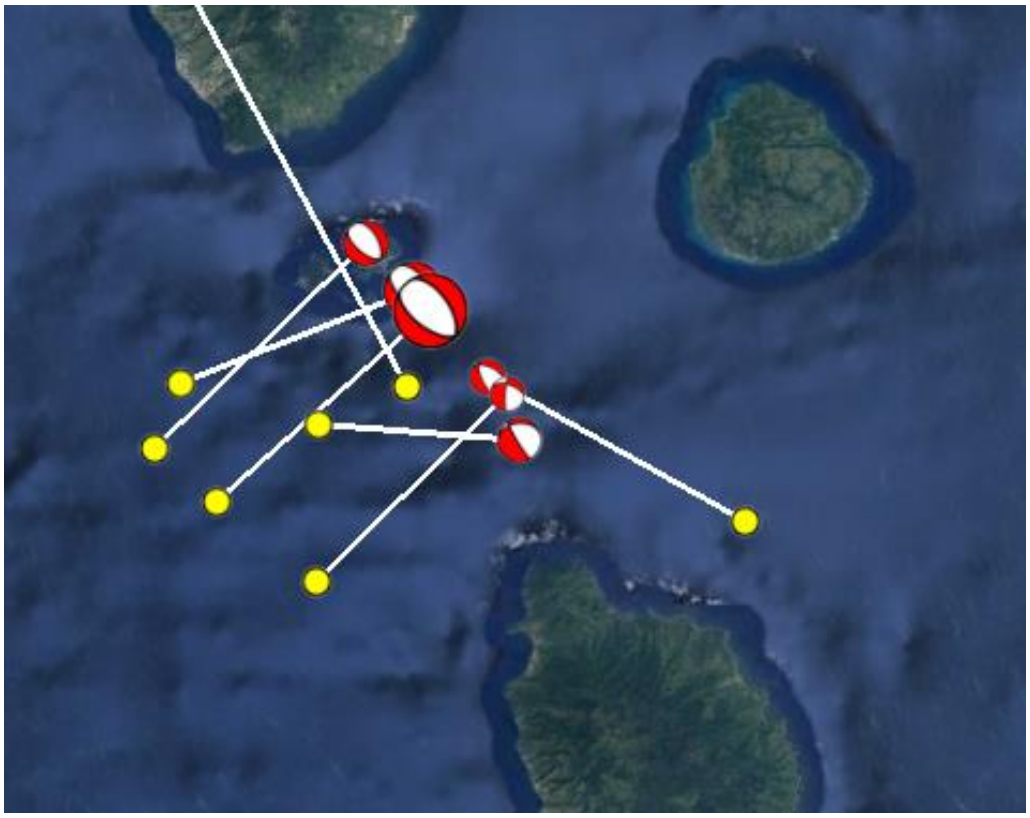

Figure 13 Cluster A

Figure 13. A map showing the six normal faulting events in cluster A. The original locations are shown as yellow circles and the relocated positions are shown as focal mechanisms that are scaled by magnitude. It is clear that the main shock is the Mw 6.3 21November 2004 event located in the middle of the cluster. The rupture then propagated along a fault oriented NW-SE evenly from the main shock. The width of the image is 75 km. Image from Google Earth.

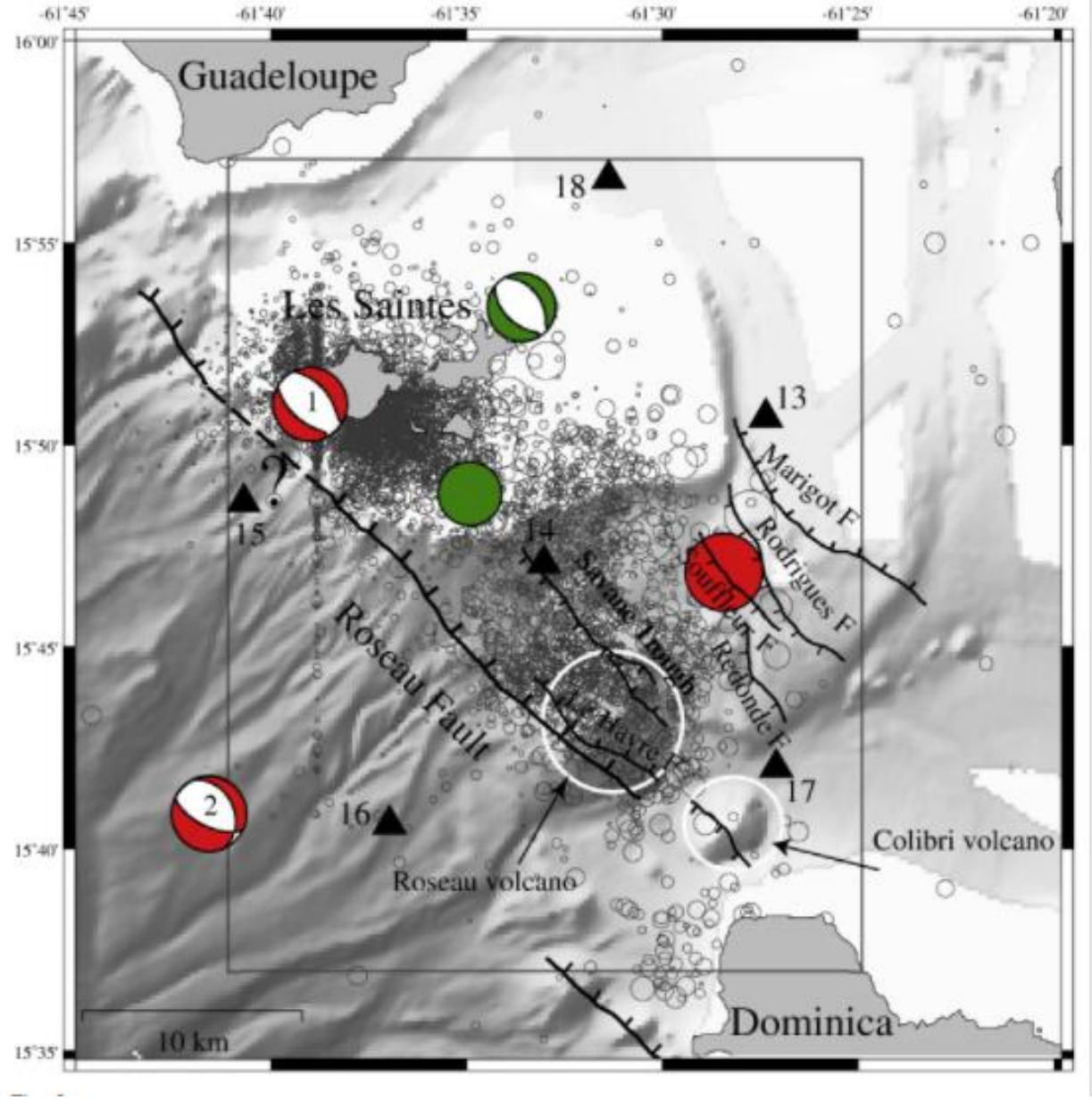

Figure 14 Roseau Fault

Figure 14. A map of the Les Saintes en echelon fault system, with the main fault being the Roseau Normal Fault. The Roseau Fault is the most likely place of the 21 November 2004 Mw 6.3 earthquake. The islands of Guadeloupe, Dominica, and Les Saintes are pictured. Aftershocks of the main event are shown as gray circles and the mainshock location predicted by Bazin et al. 2010, the relocations of this study are not shown on this map. Figure from (Bazin et al. 2010).

Bazin et al. (2010) showed that the aftershocks define a fault width (along the dip direction) of about 10 km. The aftershock distribution and our locations suggest a length of about 20 km, thus the mainshock rupture is approximately 200 km^2. This is a typical area expected for an earthquake this size. Using an empirical approximation, $Log(A) = M - 4$ (Equation 1), the expected area is 190 km^2 for a Mw 6.3 earthquake. The seismic moment of this event is $3.44x10^{18}$ N-m, so when using a shear modulus of 35 GPa and an area of 200 km^2, we find that the slip along the fault is 50 cm from the equation $M_O = \mu AD$ (Equation 2) where μ is the shear modulus, A is the area of the rupture, and D is the slip displacement.

Cluster B

Cluster B is composed of three normal faulting earthquakes that are located near the middle of the arc (Figure 15), about 25 km east of Marie Galante Island or east-southeast of Guadeloupe. These events have faulting geometry variations and are relatively deep, between 30-60 km (GCMT), and thus are susceptible to noise from variations in phase differences associated with depth variations and faulting geometry. Not surprisingly, the relocated positions show no clear faulting pattern. In general, the three events suggest that this part of the arc is complex, extension for two of the events is in the NW/SE direction, which is perpendicular to that for the other events in the region. Perhaps the stress changes approximately 50 km from the arc or the stress differences exist between the upper and lower plates.

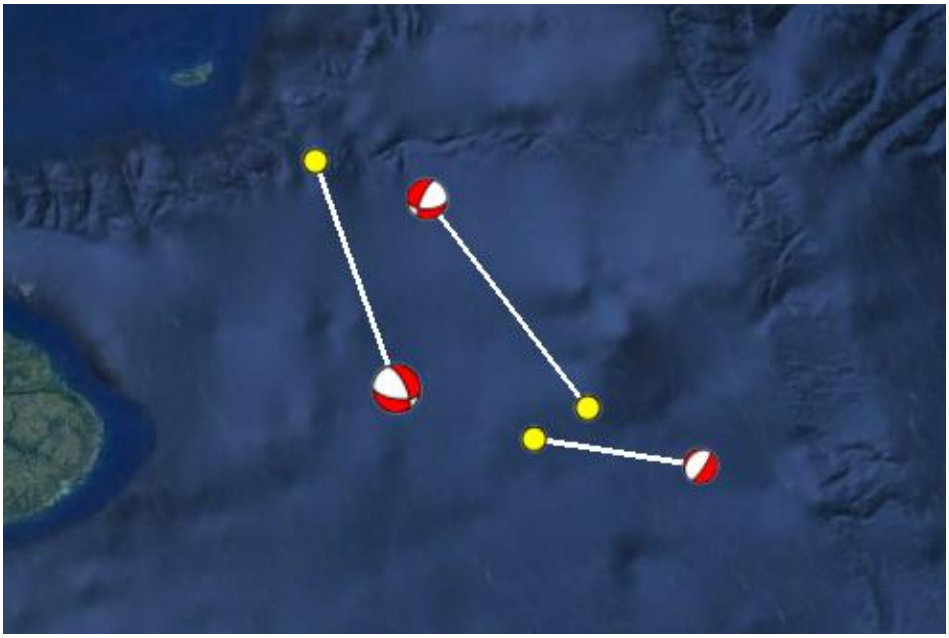

Figure 15 Cluster B

Figure 15. Cluster B relocations shown with a focal mechanism and original locations shown with a yellow circle. The white line between the points indicated the distance that the event was relocated. The focal mechanisms show a complex faulting pattern. The width of the image is 65 km. Image from Google Earth.

Cluster C

Cluster C is comprised of the strike-slip faulting events located to the northeast of the arc (Figure 16). I relocated four events, 30 March 1984, 11 July 1999, 14 May 2003, and 03 December 2011. The event farthest from the arc is the 14 May 2003 event and is also the deepest, with a depth of 40 km. The three events closer to the arc are shallower, 12 km, 10 km, and 15 km. After relocation, the four events do not align along a single fault. The compression and tension axes are generally compatible and suggest that the regional stress field in this part of the North Atlantic has NE/SW oriented compression and NW/SE oriented tension. Three of the events have moderate magnitudes of about Mw 5.5, the 14 May 2003 event is a Mw 6.6, and is located about 130 km from the trench. Despite it's size, the 2003 earthquake had no detectable aftershock sequence. Weak aftershock sequences are a characteristic common to many earthquakes in the oceanic lithosphere (Boettcher & Jordan 2004). Although no simple pattern emerged from the four events, they are likely associated with transform faults formed near the Mid Atlantic Ridge. Bergman et al (1986) discusses intraplate earthquakes to the east of the Lesser Antilles Arc and a diffuse band of seismicity that extends from the northern portion of the arc to the Mid Atlantic Ridge. This diffuse band intersects the ridge at a major left-lateral offset and the strikes of the earthquakes are roughly parallel to the transform faults in this region. Their conclusion is that the fault surface is striking WNW and this would align with the theory that they are rupturing along a fracture zone made of old transform faults (Bergman 1986). Considering the fault orientations and relative locations, the faults strike in similar directions but do not align in any simple structure, or show a simple east-to-west progressing structure. The locations suggest an overlapping, diffuse deformation zone associated with the plate boundary extending from the direction of the Mid Atlantic Ridge into the Lesser Antilles region.

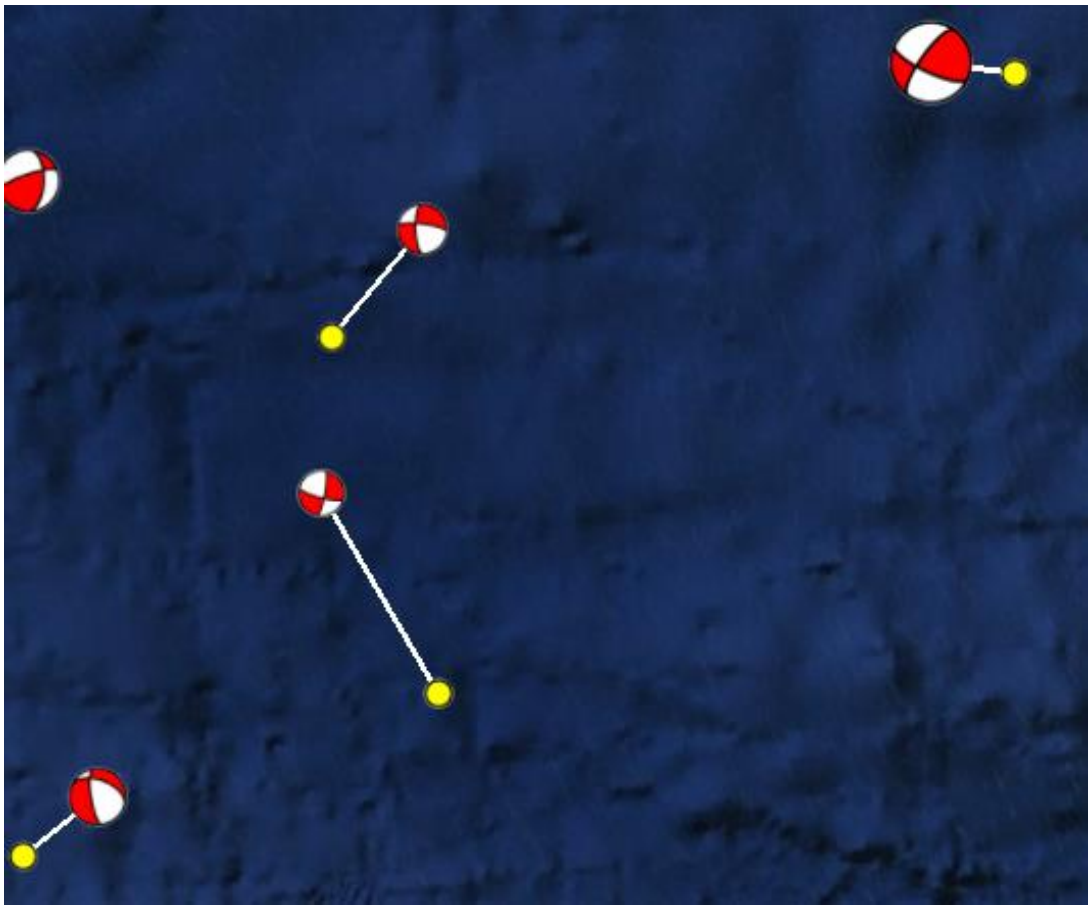

Figure 16 Cluster C

Figure 16. Cluster C contains four strike-slip faulting events that have compressional axes located in the NW-SE direction. These events are most likely located on old transform faults from the Mid Atlantic Ridge. The width of the image is ~200 km. Image from Google Earth.

Cluster D

Cluster D contains a collection of reverse faulting earthquakes and likely represents the seismogenic zone of the subduction zone (Figure 17). The cluster is located between 16N and 18N and -62W and -60W. The strike of the reverse faulting plane generally parallels the arc and starts ~50 km from the main arc. These events occur at a variety of depths between 15 km and 50 km, with the deeper events closest to the trench. Damage reports on surrounding islands suggest that the large, Mw 7.5-8.5 1843 earthquake occurred in this region. Hayes et al. (2013) estimated that less than 15% of the potential plate motion has been released seismically in this region since 1900. The implication is that 80% or more of plate motion is likely accumulating as strain and could fail in a major earthquake (Hayes et al. 2013). Summing the seismic moment of the reverse faulting events I analyzed in the region totals only about $6x10^{18}$ N-m, equivalent to a ~Mw 6.5, which is trivial compared to the Mw 7.5-8.5 estimated for the 1843 earthquake. Just south of this cluster, to the east of Guadeloupe, is a region of relative quiescence and no earthquakes greater than Mw 4.8 have occurred here since 1982. Dorel et al. (1981) described this region as a seismic gap, meaning that there are only small earthquakes and that this segment of the subduction zone may be completely locked (Dorel 1981). The key point is that the region of the large events in the 1800's appear to be accumulating strain and are thus capable of hosting significant future earthquakes. The relocations change the relationships between individual nearby events, but overall, the subduction boundary seismicity is composed of small asperity failure spread across the interface. The seismogenic zone appears to extend almost beneath the easternmost islands in the Lesser Antilles, from Barbuda to Guadeloupe. The fault slip directions are compatible with slightly oblique subduction and in agreement with the plate convergence direction described earlier in Figure 2.

Figure 17 Cluster D

Figure 17. Relocations of Cluster D shown as focal mechanisms and original locations are shown as yellow circles. These events are shallowly dipping and represent the main seismogenic region of the subduction zone. The width of the image is ~300 km. Image from Google Earth

Cluster E

Cluster E is located from the islands towards the east near approximately 14N latitude and contains eight strike-slip faulting earthquakes and four normal faulting earthquakes (Figure 18). Two of these earthquakes will be examined in Cluster Ei due to their similarities. The other 10 events range from magnitude 4.9 to 6.4 and occur over a period of 27 years. The 12 July 1990 event is located closest to the trench and is deeper than most of the other events, and has compressional and tension axes in different orientations than the other events. The 1990 compressional axis is orientated E/W, the other events in this cluster have compressional axes orientated approximately N/S. The difference suggests a change in stress seaward from the arc. This is not a completely uniform pattern, however, due to a shallow event (GCMT depth of 5 km) from 2014 that exhibits a northeast-southwest compression, similar to strike-slip events to the east, but is located closer to the arc. The variation in stress axes of the other events suggests that the stresses near the arc are east-west compression, but farther east stresses change to N/S compression. This is also seen in cluster C, in which all of the strike-slipping events are located farther east of the trench and have compressional stresses generally oriented N/S.

The relatively large Mw 6.4 (Mo = 5.91×10^{18} N-m) 18 March 2014 event had few detectable aftershocks (Figure 19 shows the small amount of seismicity associated with this event). This is similar to the Mw 6.6 14 March 2003 and again consistent with observations that earthquakes in the oceanic lithosphere exhibit fewer aftershocks than their counterparts in arc and continental regions and along subduction plate boundaries. These two events occurred far to the east of the islands, but such events can pose a hazard if the strain release that produced them continues as the plate subducts and moves closer to populated regions.

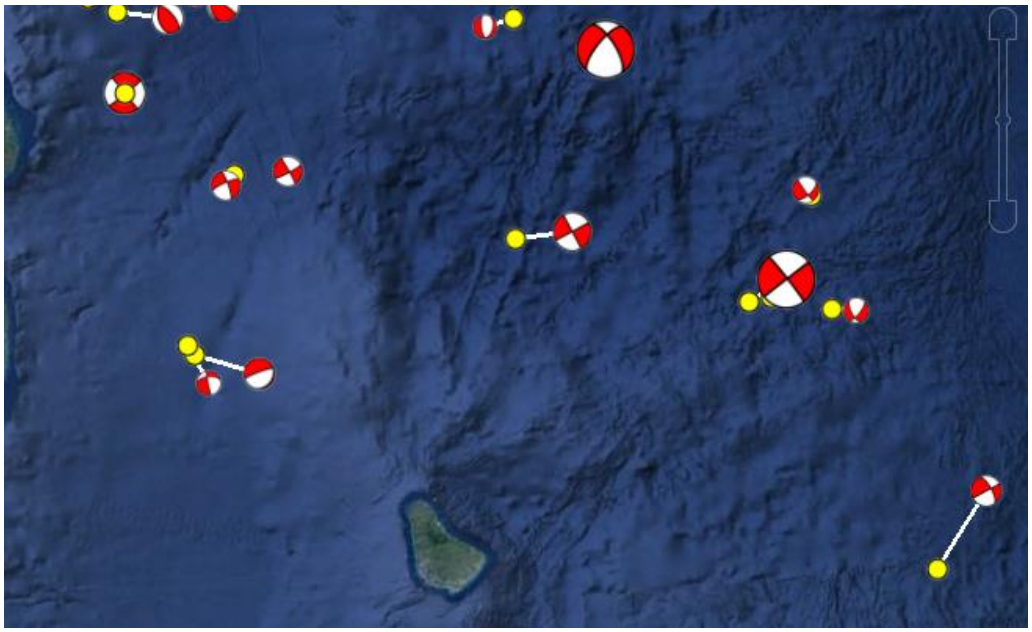

Figure 18 Cluster E

Figure 18. Cluster E relocations shown as focal mechanisms and original locations shown as yellow circles. These earthquakes show a stress change from the west to the east due to their changing P/T axes orientations, which is most likely a consequence of moving from the upper plate to the lower plate. The width of the image is ~300 km. Image from Google Earth.

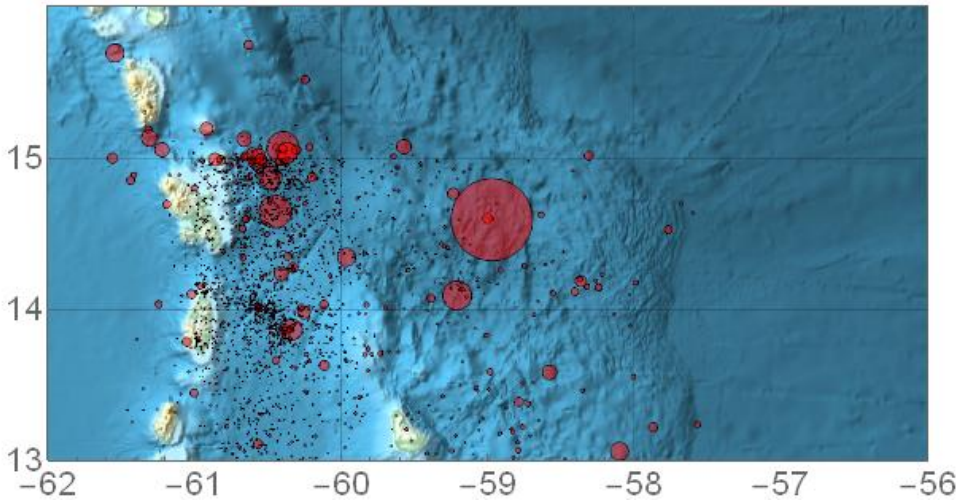

Figure 19 Cluster E region with earthquakes M > 2

Figure 19. M > 2 earthquakes associated the events in cluster E. The large circle represents the 14 March 2014 earthquake and there are few smaller earthquakes or aftershocks in the vicinity of this event. Data source: The International Seismic Centre (ISC).

Cluster Ei

Cluster Ei contains two strike-slip events that occurred on the same day, 16 July 2015, about five kilometers apart (Figure 20). The smaller, Mw 5.7 event appears to be a foreshock to the Mw 6.5. A one-kilometer shift of the smaller event would align the two events along the NW-SE plane in the GCMT catalog, a two-kilometer shift would align them along the NE-SW plane, so we cannot use the data to identify the fault plane. The spatially close epicentroids suggests that the larger earthquake may have ruptured bilaterally (assuming that the foreshock was close to the mainshock hypocenter).

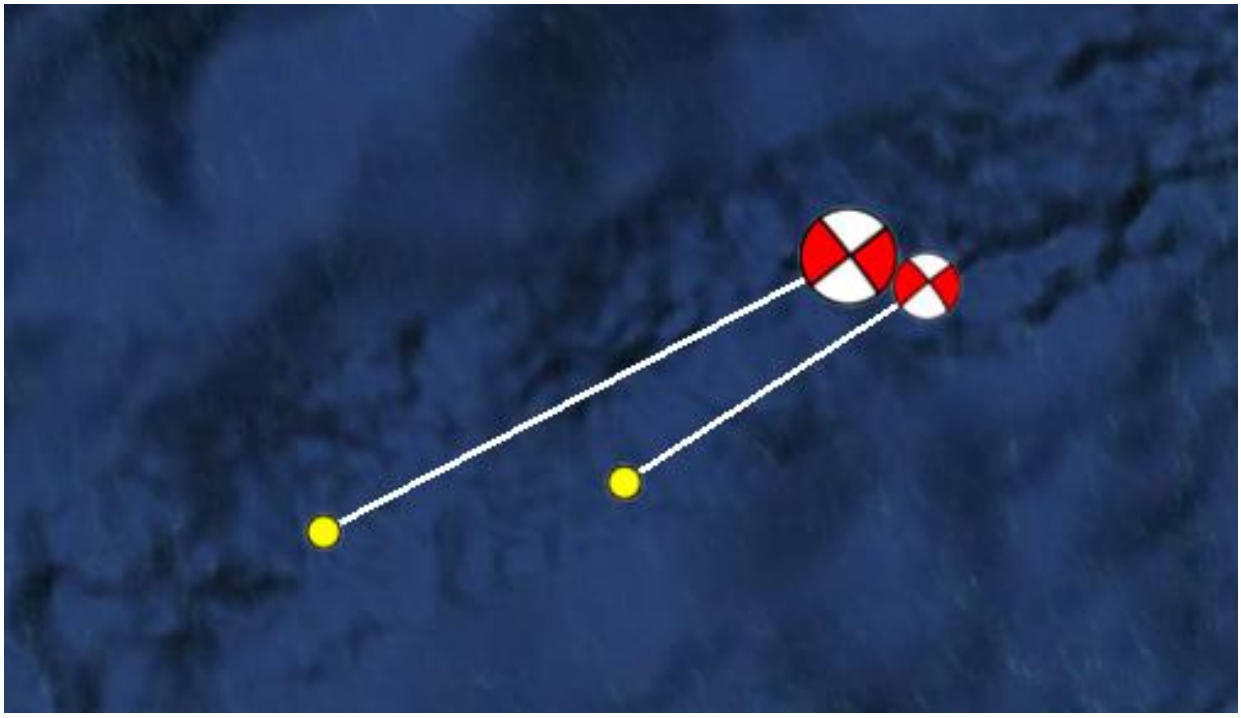

Figure 20 Cluster Ei

Figure 20. Cluster Ei, showing the en echelon nature of this fault system, with the location of the fault plane unable to be identified from the relocations. The width of the image is ~45 km. Image from Google Earth.

Cluster F

Two strike-slip faulting events, southeast of Charleston and east of Redondo, occurred on 16 March 1985 and 12 February 1986 and had magnitudes of Mw 6.3 and Mw 5.6 and depths of 14 km and 15 km, respectively (Figure 21). The long time between the events makes it uncertain if this is a simple aftershock relationship, but the proximity of these events and their similar strike suggests that they have ruptured along the same fault. As with the 2015 events described above, roughly two-kilometer shifts can align the two events along either plane, so we cannot identify the strike of the structure. But we can say that the event centroids are only a few kilometers apart. Figure 22 shows the aftershocks of the 16 March 1985 event. The aftershocks do not rupture along a single line, so we cannot use them to define a faulting surface. The shallow depths suggest that they are located in the overriding plate. The focal mechanisms suggest approximately E/W compression, compatible with stress induced as a result of the plate convergence. The surface-wave epicentroids appear to be shifted substantially from the regional locations, which may be an indication of variation in slowness (that can affect my absolute locations). The relative locations would not be affected by this bias, however. More work is needed to resolve this specific issue. They key result from the surface-waves is that the centroids are close.

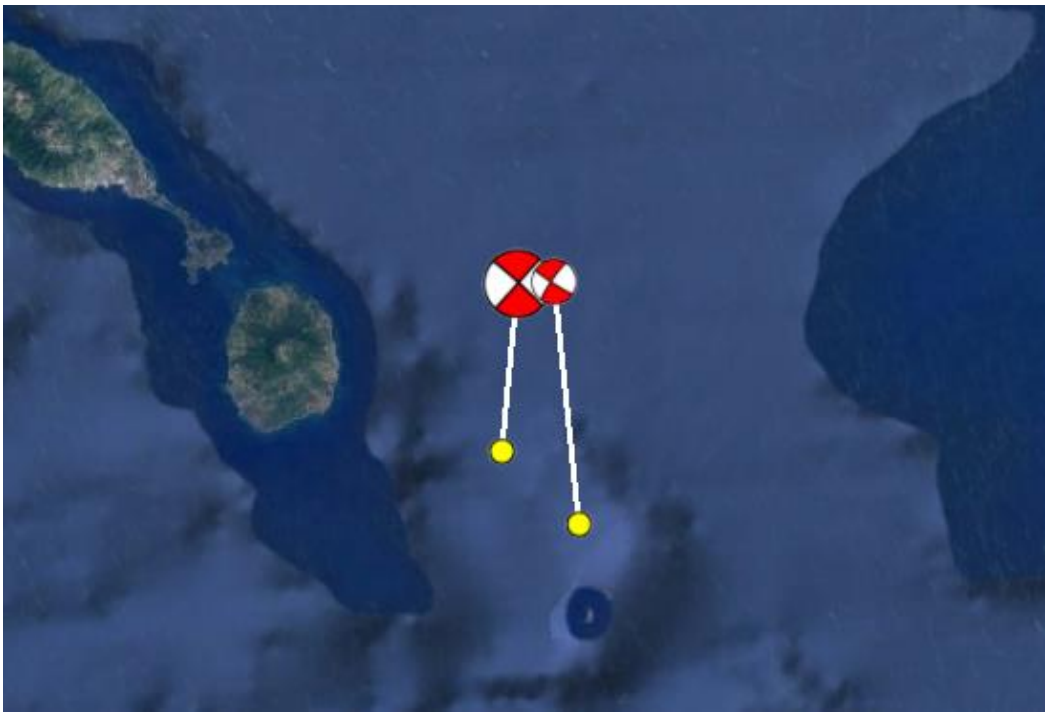

Figure 21 Cluster F

Figure 21. This cluster is located in the northern region of the arc. The fault plane cannot be determined from the surface waves. The compressional axis is in the E-W direction. Because the fault planes do not line up, this system can be characterized as an en echelon. The width of the image is ~80 km. Image from Google Earth.

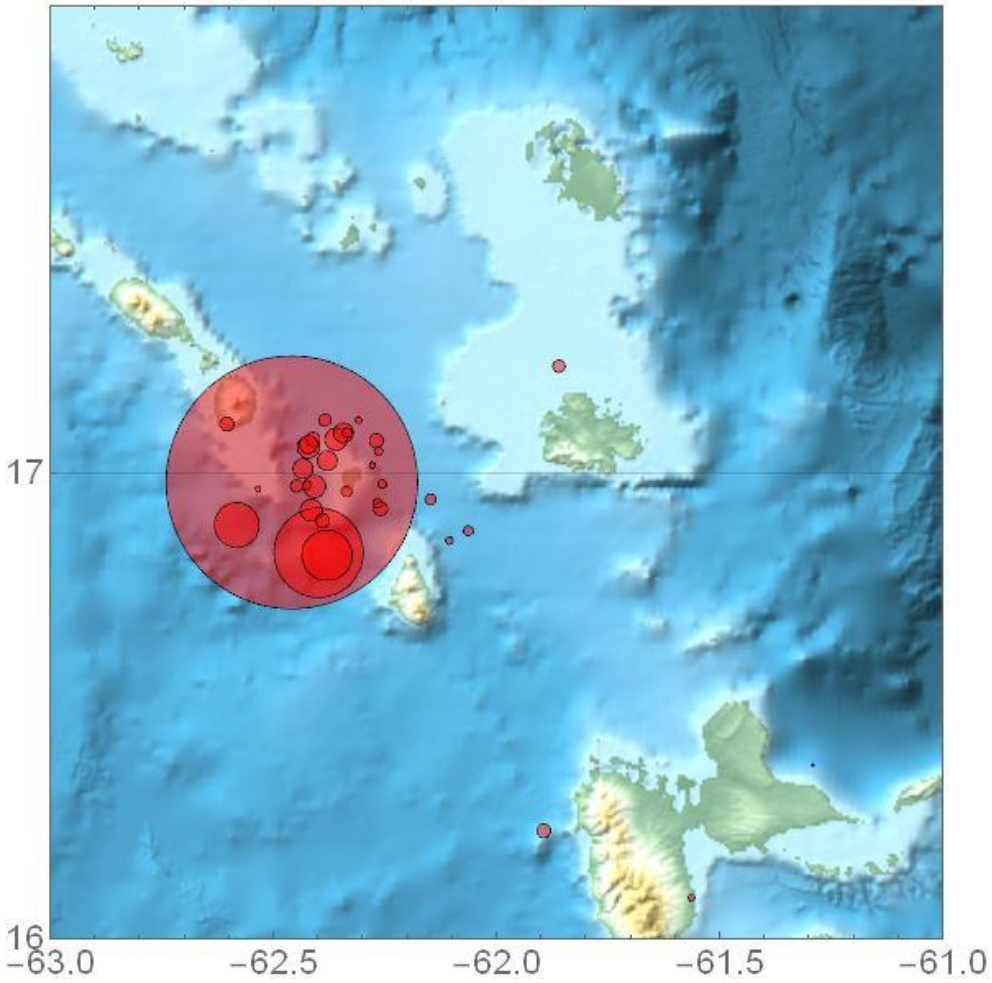

Figure 22 Aftershocks of 16 March 1985 earthquake

Figure 22. Aftershocks of the Mw 6.3 16 March 1985 event in Cluster F, denoted as the largest circle. The aftershocks shown are M >2 and from a month after the event.

Cluster G

Cluster G consists of five reverse faulting events that are located just north and 50-150 km east of Martinique (Figure 23). All have relatively similar magnitudes, ranging from Mw 4.9-5.3 and none are clearly part of an aftershock sequence. The depths are mostly above 30 km and the 21 November 1988 event is located at 15 km depth (fixed) and is located in the middle of the sequence. The focal mechanisms vary substantially, indicating that this is a region of complicated faulting but compression is generally east-west or northeast-southwest. The three events closest to the trench were relocated much closer to one another, but do not show a clear faulting pattern. The shallow depths and the steepness of the potential fault planes suggest that these reverse events may not have occurred along the plate boundary.

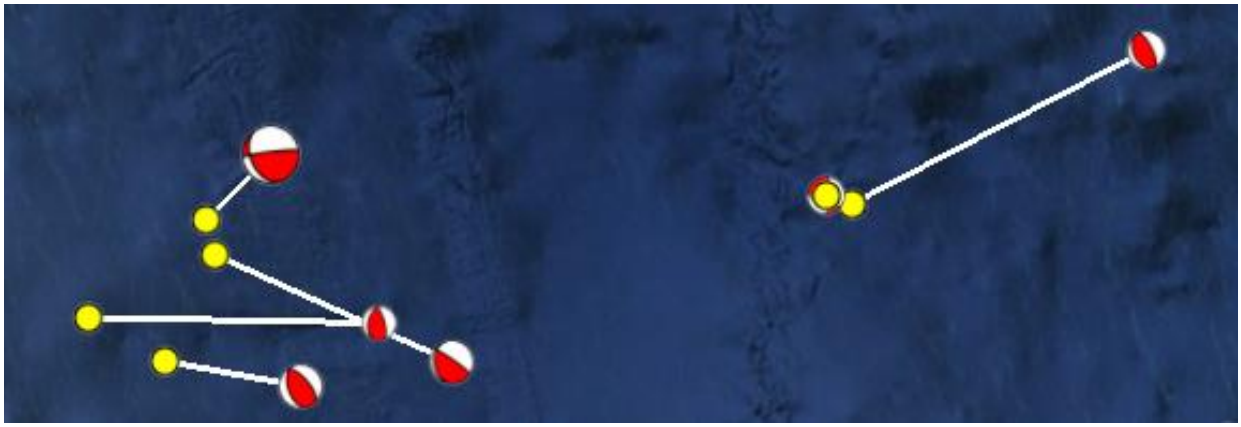

Figure 23 Cluster G

Figure 23. Cluster G, located in the southern portion of the arc. This region is complex, having focal mechanisms with P and T axes in multiple directions. The width of the image is ~160 km. Image from Google Earth.

Cluster H

Cluster H contains the four oblique, low-angle reverse faulting events in the northernmost portion of the arc, east of the Virgin Islands and north of Anguilla (Figure 24). Two of these events are from a sequence on 09 February 1988 that form a doublet, occurring 7 hours apart and located at the same depth and magnitude, 15 km and Mw 5.4. The associated seismicity is shown in Figure 25.

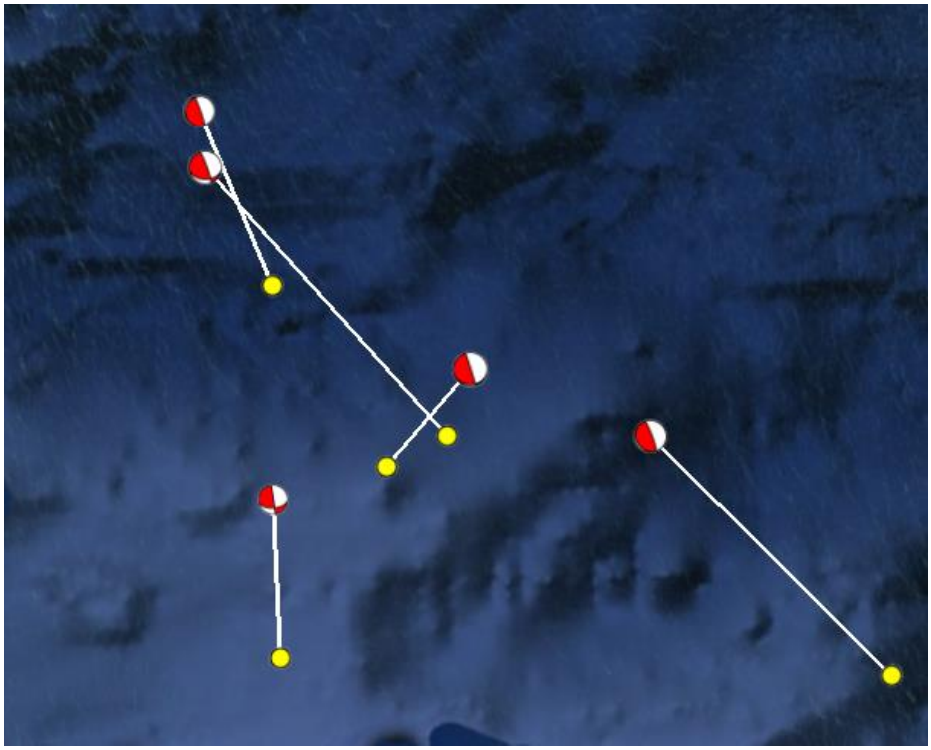

Figure 24 Cluster H

Figure 24. Cluster H located in the most northern portion of the arc. This shows that the fault plane is in the SES direction. The width of the image is ~130 km. Image from Google Earth.

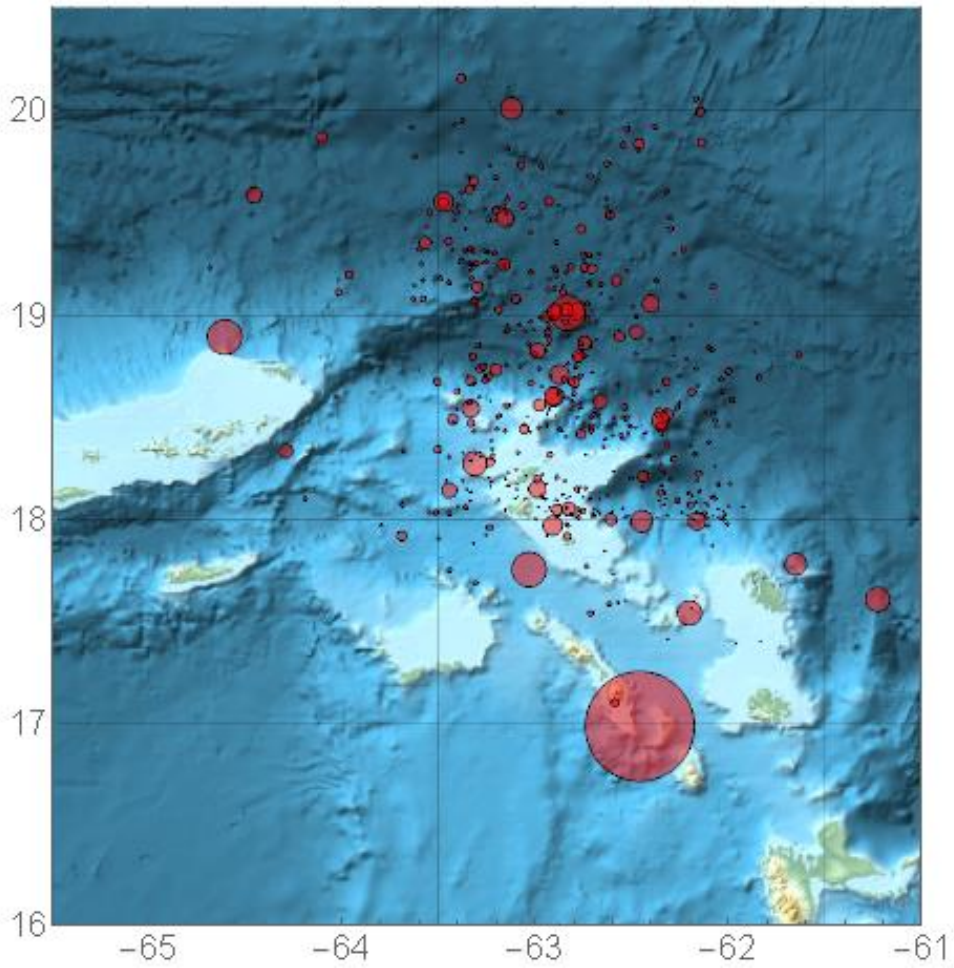

Figure 25 Cluster H region with earthquakes M >2

Figure 25. Cluster H with associated M >2 earthquakes. This shows the relatively small amount and small magnitude of seismicity in this portion of the arc.

Chapter 8

Conclusion

The Lesser Antilles Arc and Subduction Zone is a region with a significant seismic hazard. The relatively slow convergence of the North and South American Plates beneath the eastern Caribbean Plate have produced a modest number of shallow seismic activity during the 35 years addressed in this study. Two large earthquakes in the 1800's point to a large earthquake potential in the region, which appears to have released only about 10% of the potential seismic strain accumulating since the large earthquakes. The sparse nature of the seismicity makes mapping the hazard somewhat of a challenge. Recent damaging earthquakes are associated with faulting within the upper plate, which shows extension in the arc (e.g. the 2004 Les Saintes earthquake) and east-west driven strike slip faulting in the upper plate east of the arc. Surface-wave relocation and examination of the GCMT faulting patterns of the moderate-magnitude events has revealed several interesting relationships. The Les Saintes earthquake sequence of 2004 is compatible to a rupture along Roseau fault, in length and azimuth, located between Dominica and Les Saintes Islands; the southern half of the rupture shows more faulting heterogeneity and is coincident with a region of en echelon faulting. Moderate-magnitude low angle reverse faulting events are located in the seismogenic zone of the subduction zone, where the segment of the megathrust is believed to have failed during the large 1843 earthquake. The seismogenic zone appears to extend very close to the easternmost islands in the chain. The large strike-slip earthquakes that occurred within the down-going plate(s) show characteristics common with earthquakes in the oceanic lithosphere, notably a low number of detected

aftershocks. One of these events had a moderate-magnitude foreshock, another an aftershock, and both were located within a few kilometers of the mainshock spatial centroid. The strike-slip events suggest a ~N-S, NW-SE oriented compressive stress within the subducting plates, which may suggest some compression between the North and South American Plates. The boundary between these plates remains elusive since the deformation appears to spread over several hundred kilometers seaward of the trench. East of the arc, within the overriding plate, there is evidence for east-west compression (likely caused by subduction) and within the arc, the normal faulting of the Les Saintes earthquake indicated roughly east-west extension. Given the increases in permanent and tourist-related populations in the region, continued work to unravel the seismic hazards in the region will remain important into the future.

Appendix A

Body-Waveform Modeling Depth Estimates

Date of Earthquake	Longitude	Latitude	Original Depth	Estimated Depth
2008-02-06-18-37-59	-60.132	14.876	30	34.7
2016-03-19-11-26-37	-60.309	18.174	38	32.1
2016-02-02-07-18-37	-60.217	14.921	44	33
2015-09-29-18-49-40	-58.203	13.82	12	24.6
2013-07-08-09-14-17	-61.57	18.307	37	42.3
2007-02-27-09-42-42	-61.52	17.053	50	62.3
2004-03-30-16-23-35	-62.192	17.494	44	39
2002-12-21-18-50-55	-62.64	18.629	31	18
2002-10-01-07-00-58	-63.134	19.001	15	23.2
2001-12-07-15-59-53	-61.045	16.858	28	28
2001-09-25-23-16-59	-61.379	17.065	35	23.2
2000-10-30-03-07-14	-61.16	17.512	22	33.3
2000-10-27-19-02-55	-61.141	17.531	18	42
2000-02-16-07-03-13	-60.785	17.836	15	33.5
1998-06-25-21-03-46	-61.554	17.619	27	16
2000-02-23-19-20-32	-60.653	17.488	28	33.2
1994-08-15-06-15-43	-60.647	16.74	18	40
1994-07-23-07-22-07	-61.261	16.755	41	36.4
1991-12-30-22-38-01	-61.557	17.589	49	52

Appendix B

Surface-Wave Based Relocations

The bolded rows within each table show the events that were relocated using the surface wave cross-correlation method.

Normal Faulting Earthquake Relocations

Date of Earthquake	Original Longitude	Original Latitude	Relocated Longitude	Relocated Latitude	Magnitude
1992-08-03-02-53-54	-60.95	16.08	-60.95	16.08	5.4
1995-03-08-03-46-04	-59.56	16.59	-59.56	16.59	6.1
1999-06-08-12-04-04	**-60.24**	**15.06**	**-60.343**	**15.113**	**5.8**
2001-01-05-08-06-37	**-61.03**	**16.11**	**-60.978**	**15.949**	**5.7**
2001-04-05-13-54-24	**-60.98**	**16.06**	**-60.76**	**15.886**	**5.1**
2003-06-30-00-07-28	**-61.29**	**17.28**	**-61.594**	**17.705**	**5.7**
2004-03-01-06-12-09	-60.74	15.16	-60.74	15.16	4.8
2004-11-21-11-41-12	**-61.65**	**15.85**	**-61.542**	**15.828**	**6.3**
2004-11-21-13-37-01	-61.47	15.73	-61.47	15.73	5.3
2004-11-21-18-53-04	**-61.56**	**15.89**	**-61.594**	**15.879**	**5.3**
2004-11-27-23-44-25	**-61.49**	**15.77**	**-61.48**	**15.765**	**4.9**
2004-12-02-14-47-57	**-61.54**	**15.83**	**-61.496**	**15.778**	**5**
2005-02-14-18-06-03	**-61.56**	**15.89**	**-61.556**	**15.843**	**5.8**
2005-06-06-01-20-08	-61.79	16.16	-61.79	16.16	4.8
2006-10-08-10-06-43	-59.31	14.76	-59.31	14.76	4.8
2011-08-07-04-01-10	-60.09	13.75	-60.09	13.75	5.3
2014-02-18-09-27-18	**-58.92**	**14.74**	**-58.936**	**14.667**	**6.4**
2014-05-16-11-01-47	-60.24	17.18	-60.24	17.18	5.9
2015-09-29-18-49-40	**-58.22**	**13.75**	**-58.203**	**13.82**	**4.9**

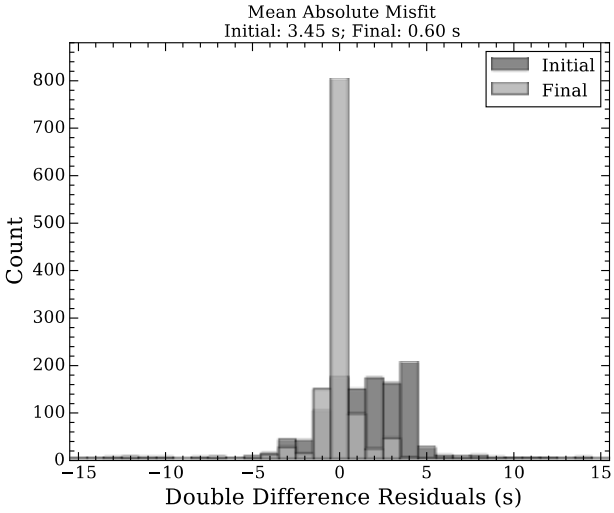

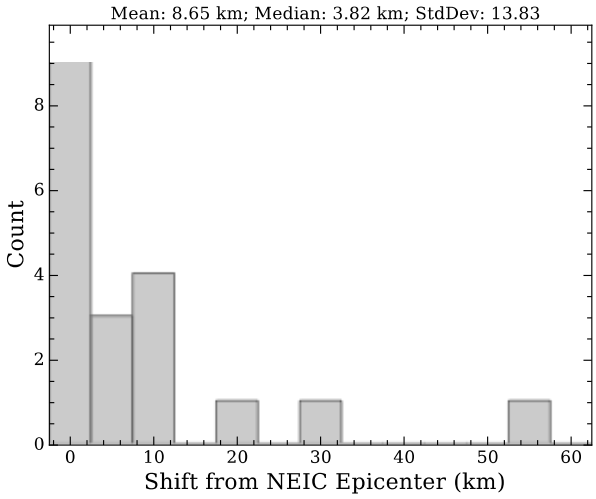

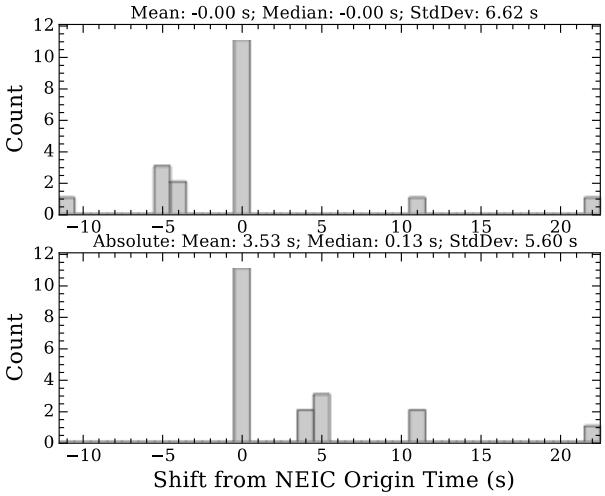

Histograms showing the statistics of the normal-faulting earthquake relocations. Each histogram is labeled and details are outlined in the results.

Reverse Faulting Earthquake Relocations

Date of Earthquake	Original Longitude	Original Latitude	Relocated Longitude	Relocated Latitude	Magnitude
1982-01-30-02-35-13	-61.47	16.71	-61.47	16.71	6
1983-03-03-11-53-17	-60.31	14.85	-60.31	14.85	5.3
1983-04-05-15-59-41	-61.58	17.29	-61.58	17.29	5.1
1985-11-28-00-14-05	-60.95	12.1	-60.95	12.1	5.5
1986-11-09-22-27-31	-60.84	17.35	-60.84	17.35	5
1988-02-09-02-22-32	-63.13	18.94	-63.13	18.94	5.4
1988-02-09-19-12-47	-62.84	18.71	-62.84	18.71	5.4
1988-04-22-04-03-37	-61.34	17.18	-61.34	17.18	5.1
1988-11-21-05-19-18	-59.69	15.06	-59.69	15.06	5
1989-03-11-19-31-24	-60.82	17.37	-60.82	17.37	5.1
1991-02-05-23-34-31	-61.46	17.31	-61.46	17.31	5.2
1991-12-30-22-38-01	**-61.14**	**17.78**	**-61.557**	**17.589**	**5.3**
1994-07-23-07-22-07	**-61.11**	**16.76**	**-61.261**	**16.755**	**5.4**
1994-08-15-06-15-43	**-60.76**	**16.81**	**-60.647**	**16.74**	**5.4**
1995-06-30-07-47-29	**-61.39**	**17.51**	**-61.452**	**17.656**	**5.4**
1998-06-25-21-03-46	**-61.67**	**17.75**	**-61.554**	**17.619**	**5.6**
1999-08-28-04-27-51	**-61.46**	**16.95**	**-61.438**	**17.042**	**5.3**
2000-02-16-07-03-13	**-61**	**17.92**	**-60.785**	**17.836**	**5.3**
2000-02-23-19-20-32	**-60.43**	**17.37**	**-60.653**	**17.488**	**5.4**
2000-10-27-19-02-55	**-61.24**	**17.76**	**-61.141**	**17.531**	**5.6**
2000-10-30-03-07-14	**-61.23**	**17.46**	**-61.16**	**17.512**	**5.8**
2001-09-25-23-16-59	**-61.36**	**17.17**	**-61.379**	**17.065**	**5.4**
2001-12-07-15-59-53	**-60.87**	**16.89**	**-61.045**	**16.858**	**5.1**
2002-10-01-07-00-58	**-63.14**	**18.54**	**-63.134**	**19.001**	**5.2**
2002-12-21-18-50-55	**-62.26**	**18.14**	**-62.64**	**18.629**	**5.3**
2004-03-30-16-23-35	**-62.24**	**17.61**	**-62.192**	**17.494**	**4.9**
2007-02-27-09-42-42	**-61.4**	**17.18**	**-61.52**	**17.053**	**5**
2008-02-06-18-37-59	**-60.32**	**15.1**	**-60.132**	**14.876**	**5.3**
2009-11-28-08-18-36	-59.31	15.22	-59.31	15.22	5
2010-05-07-23-12-12	**-60.88**	**16.56**	**-61.024**	**16.502**	**5.2**
2013-07-08-09-14-17	**-61.58**	**18.24**	**-61.57**	**18.307**	**5.1**
2016-02-02-07-18-37	**-60.57**	**15.08**	**-60.217**	**14.921**	**4.9**
2016-03-19-11-26-37	**-60.71**	**18.06**	**-60.309**	**18.174**	**6**

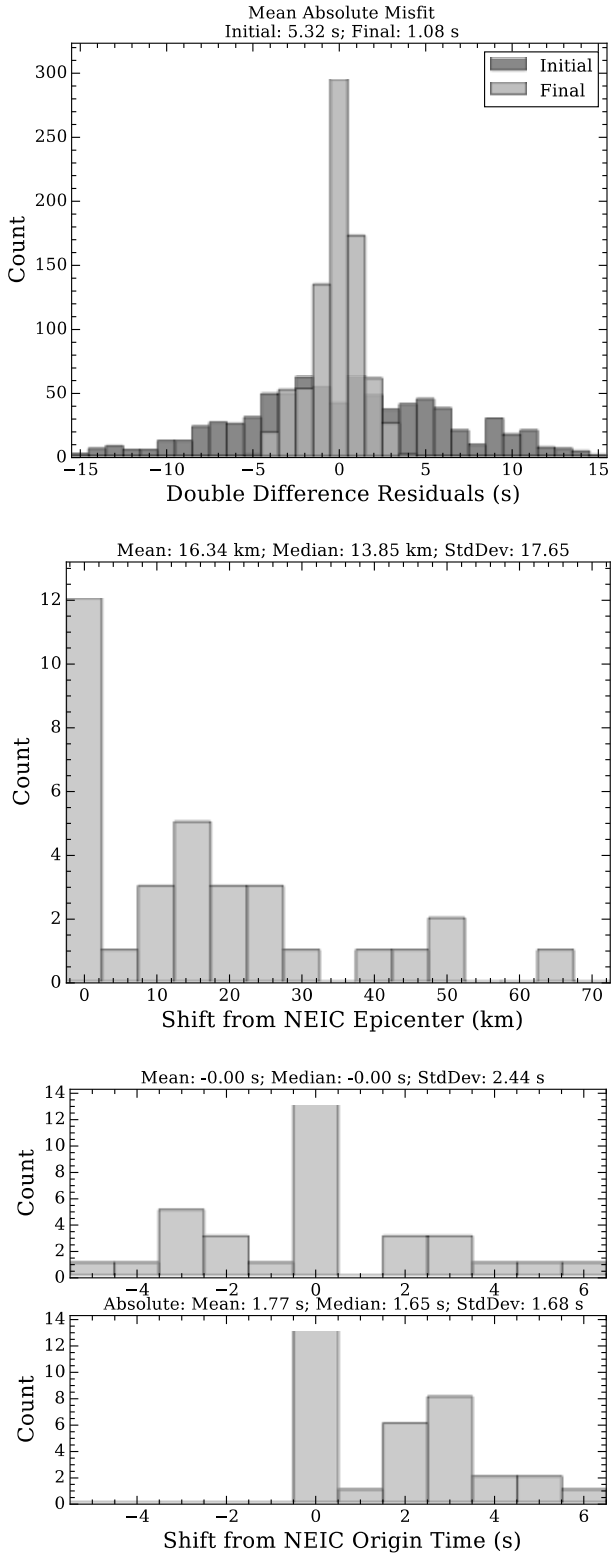

Histograms showing the statistics of the reverse-faulting earthquake relocations. Each histogram is labeled and details are outlined in the results.

Strike Slip Faulting Earthquake Relocations

Date of Earthquake	Original Longitude	Original Latitude	Relocated Longitude	Relocated Latitude	Magnitude
1984-03-30-07-59-57	-59.84	17.65	-59.84	17.65	5.4
1985-03-16-14-54-04	**-62.34**	**17.1**	**-62.39**	**17.2**	**6.3**
1985-07-05-06-17-18	-63.07	18.58	-63.07	18.58	5.2
1986-02-12-23-41-46	**-62.41**	**17.3**	**-62.36**	**17.2**	**5.6**
1987-08-12-03-10-00	-59.08	14.12	-59.08	14.12	5.6
1990-07-12-23-08-25	-60.46	14.63	-60.46	14.63	5.8
1995-12-29-14-36-54	-59.31	14.39	-59.31	14.39	5.2
1999-07-11-11-51-19	-60.32	16.9	-60.32	16.9	5.2
2003-05-14-06-03-38	**-58.72**	**18.29**	**-58.772**	**18.294**	**6.6**
2006-06-11-00-24-34	**-58.33**	**14.3**	**-58.336**	**14.198**	**5**
2011-12-03-09-27-15	**-59.7**	**18.07**	**-59.648**	**18.066**	**5.6**
2012-12-27-05-36-14	**-57.85**	**13.15**	**-57.828**	**13.238**	**5.2**
2014-09-15-21-09-11	**-60.14**	**14.34**	**-60.158**	**14.329**	**5.2**
2014-12-07-15-35-48	**-60.27**	**13.72**	**-60.251**	**13.731**	**4.9**
2015-07-16-11-01-49	**-58.43**	**13.89**	**-58.399**	**13.923**	**5.7**
2015-07-16-15-16-38	**-58.37**	**13.95**	**-58.417**	**13.93**	**6.5**

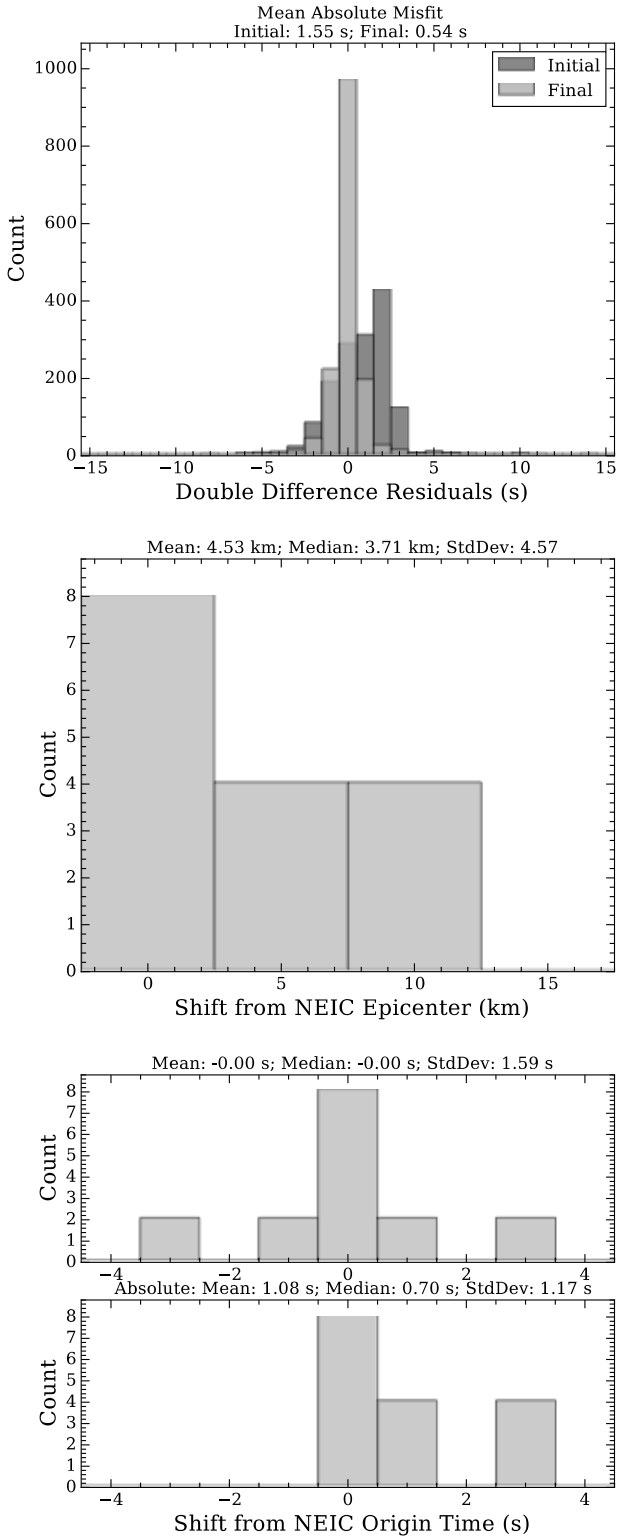

Histograms showing the statistics of the strike-slip faulting earthquake relocations. Each histogram is labeled and details are outlined in the results.

BIBLIOGRAPHY

Bazin S, Feuillet N, Duclos C, Crawford W, Nercessian A, et al. 2010. The 2004–2005 Les Saintes (French West Indies) seismic aftershock sequence observed with ocean bottom seismometers. *Tectonophysics*. 489(1–4):91–103

Bergman EA. 1986. Intraplate earthquakes and the state of stress in oceanic lithosphere. *Tectonophysics*. 132(1):1–35

Bernard P, Lambert J. 1988. Subduction and seismic hazard in the northern Lesser Antilles: Revision of the historical seismicity. *Bull. Seismol. Soc. Am*. 78(6):1965–83

Boettcher MS, Jordan TH. 2004. Earthquake scaling relations for mid-ocean ridge transform faults

Cleveland KM, Ammon CJ. 2013. Precise relative earthquake location using surface waves. *J. Geophys. Res. Solid Earth*. 118(6):2893–2904

DeMets C, Gordon RG, Argus DF. 2010. Geologically current plate motions. *Geophys. J. Int*. 181(1):1–80

DeMets C, Jansma PE, Mattioli GS, Dixon TH, Farina F, et al. 2000. GPS geodetic constraints on Caribbean-North America Plate Motion. *Geophys. Res. Lett*. 27(3):437–40

Dorel J. 1981. Seismicity and seismic gap in the Lesser Antilles arc and earthquake hazard in Guadeloupe. *Geophys. J. Int*. 67(3):679–95

Dziewonski AM, Anderson DL. 1981. Preliminary reference Earth model. *Phys. Earth Planet. Inter.* 25(4):297–356

Feuillet N, Beauducel F, Jacques E, Tapponnier P, Delouis B, et al. 2011a. The Mw = 6.3, November 21, 2004, Les Saintes earthquake (Guadeloupe): Tectonic setting, slip model and static stress changes. *J. Geophys. Res. Solid Earth*. 116(B10):B10301

Feuillet N, Beauducel F, Tapponnier P. 2011b. Tectonic context of moderate to large historical earthquakes in the Lesser Antilles and mechanical coupling with volcanoes. *J. Geophys. Res. Solid Earth*. 116(B10):B10308

Hayes GP, McNamara DE, Seidman L, Roger J. 2013. Quantifying potential earthquake and tsunami hazard in the Lesser Antilles subduction zone of the Caribbean region. *Geophys. J. Int*. 196(1):510–21

Krischer L, Megies T, Barsch R, Beyreuther M, Lecocq T, et al. 2015. ObsPy: a bridge for seismology into the scientific Python ecosystem. *Comput. Sci. Discov*. 8(1):014003

Laigle M, Becel A, de Voogd B, Sachpazi M, Bayrakci G, et al. 2013. Along-arc segmentation and interaction of subducting ridges with the Lesser Antilles Subduction forearc crust revealed by MCS imaging. *Tectonophysics*. 603:32–54

Langston CA, Helmberger DV. 1975. A Procedure for Modelling Shallow Dislocation Sources*. *Geophys. J. R. Astron. Soc.* 42(1):117–30

McCann WR, Sykes LR. 1984. Subduction of aseismic ridges beneath the Caribbean Plate: Implications for the tectonics and seismic potential of the northeastern Caribbean. *J. Geophys. Res. Solid Earth*. 89(B6):4493–4519

Shearer P. 2009. *Introduction to Seismology*. Cambridge New York: University Press. 2nd ed.

Stein S, Engeln JF, Wiens DA, Fujita K, Speed RC. 1982. Subduction seismicity and tectonics in the Lesser Antilles Arc. *J. Geophys. Res. Solid Earth*. 87(B10):8642–64

Stein S, Wysession M. 2003. *An Introduction to Seismology, Earthquakes, and Earth Structure*. Malden MA: Blackwell Publishing

Academic Vita of Audrey Dunham

Mobile: (607) 339-8128 ● Email: aid5334@psu.edu

EDUCATION: **The Pennsylvania State University**
College of Earth and Mineral Sciences University Park, PA
Schreyer Honors College *Class of 2017*
Bachelor of Science, Geoscience
Minor: Geophysics

RESEARCH EXPERIENCE:

Earthquake Seismology Laboratory University Park, PA
Undergraduate Researcher *January 2016-Present*

- Analyzed surface waveforms for the 2 March 2016 Wharton Basin M_W 7.8 earthquake to relocate subsequent events and evaluate the nature of the earthquake.
- Synthesized a topic and currently producing an undergraduate thesis on the seismicity of the Less Antilles Arc.
- Evaluated seismic waveforms to relocate location and depth of earthquakes.
- Advanced my skills in GMT, Linux, and SAC.

Lamont Doherty Earth Observatory, Columbia University Palisades, NY
Summer Intern *June 2016-August 2016*

- Researched the faulting mechanisms of a hypothesized ancient earthquake in Bangladesh.
- Utilized Coulomb, a program run on MATLAB, to establish an elastic dislocation model for the ancient earthquake.
- Evaluated data and designed three separate models that could have resulted in the rupture.
- Developed professionalism skills by presenting my project through a talk, poster, and paper.

Volcanology and Geodesy Lab University Park, PA
Undergraduate Researcher *January 2014- January 2015*

- Developed basic skills in Linux and Generic Mapping Tool (GMT) while gaining experience working in a research laboratory environment.
- Researched the causes and processes of deformation of the Cotopaxi Volcano in Ecuador using GPS data.
- Processed and evaluated data to make a comprehensive poster and report.

Boyce Thompson Institute of Plant Research, Cornell University Ithaca, NY
Research Assistant *September 2012- May 2016*

- Assisted post-doctorate and doctorate researchers by organizing, preparing, and completing experiments in a laboratory setting.
- Learned and carried out many different techniques used in a research lab such as autoclaving and aliquoting.
- Coordinated laboratory organization by fulfilling purchasing orders and maintaining and stocking supplies.

LEADERSHIP EXPERIENCE:

Penn State Geosciences Club University Park, PA
President, Vice President, Secretary *September 2013-Present*

- Facilitate club meetings.
- Organize faculty presentations and dinners.
- Develop and plan educational and career building activities for club members.
- Foster fellowship between members of the undergraduate, graduate, and faculty of the geoscience community.

Association for Women Geoscientists University Park, PA
Member *September 2015-Present*

- Participant in graduate-undergraduate mentorship program.
- Engage in community outreach through volunteering at the local Discovery Space.

Alpha Phi Omega Service Fraternity University Park, PA
Service-Vice President, Brother *September 2014-Present*

- Planning and participating in service events around the university and community.
- Engaging in leadership workshops and team building experiences.

109H Earthquakes and Society University Park, PA
Teaching Assistant *September 2016-Present*

- Guide students through in-class activities.
- Assist students with computational, mathematical, and theory based questions.
- Communicate scientific methods and theories to non-scientists.

AWARDS:

- Presidents' Freshman Award
- Dean's List
- Shell Oil Technical Scholarship
- Marathon Oil Honors Scholarship
- Matthew J Wilson Honors Scholarship
- College of Earth and Mineral Sciences Merit Scholarship
- Honess Memorial Award
- Schreyer American Geophysical Union Grant
- Schreyer Wellington: Victoria University Grant

PUBLICATIONS:

Lay T, Ye L, Ammon CJ, **Dunham A**, Koper KD. 2016. "The 2 March 2016 Wharton Basin Mw!7.8 earthquake: High stress drop north-south strike-slip rupture in the diffuse oceanic deformation zone between the Indian and Australian Plates", *Geophys. Res. Lett.* 43(15):2016GL069931

PRESENTATIONS:

Dunham, A., "Complex Channel Avulsion in the Meghna River Floodplain During the Mid to Late Holocene: The Potential Effect of Tectonic and Co-Seismic Uplift", poster presented at the American Geophysical Union Fall Meeting 2016 in San Francisco, California.